Published in final edited form as:

J Physiol. 2021 May ; 599(10): 2673–2697. doi:10.1113/JP279024.

Structure and Function of the calcium-selective TRP channel TRPV6

Maria V. Yelshanskaya[1], **Kirill D. Nadezhdin**[1], **Maria G. Kurnikova**[2], **Alexander I. Sobolevsky**[1]

[1]Department of Biochemistry and Molecular Biophysics, Columbia University, 650 West 168th Street, New York, NY 10032

[2]Chemistry Department, Carnegie Mellon University, 4400 Fifth Ave., Pittsburgh, PA, 15213

Abstract

Epithelial calcium channel TRPV6 is a member of the vanilloid subfamily of TRP channels that is permeable to cations and highly selective to Ca^{2+}; it shows constitutive activity regulated negatively by Ca^{2+} and positively by phosphoinositol and cholesterol lipids. In this review, we describe the molecular structure of TRPV6 and discuss how its structural elements define its unique functional properties. High Ca^{2+} selectivity of TRPV6 originates from the narrow selectivity filter, where Ca^{2+} ions are directly coordinated by a ring of anionic aspartate side chains. Divalent cations Ca^{2+} and Ba^{2+} permeate TRPV6 pore according to the knock-off mechanism, while tight binding of Gd^{3+} to the aspartate ring blocks the channel and prevents Na^{+} from permeating the pore. The iris-like channel opening is accompanied by an α-to-π helical transition in the pore-lining transmembrane helix S6. As a result of this transition, the intracellular halves of the S6 helices bend and rotate by about 100 degrees, exposing different residues to the channel pore in the open and closed states. Channel opening is also associated with changes in occupancy of the transmembrane domain lipid binding sites. The inhibitor 2-aminoethoxydiphenyl borate (2-APB) binds to TRPV6 in a pocket formed by the cytoplasmic half of the S1-S4 transmembrane helical bundle and shifts open-closed channel equilibrium towards the closed state by outcompeting lipids critical for activation. Ca^{2+} inhibits TRPV6 via binding to calmodulin (CaM), which mediates Ca^{2+}-dependent inactivation. The TRPV6-CaM complex exhibits 1:1 stoichiometry; one TRPV6 tetramer binds both CaM lobes, which adopt a distinct head-to-tail arrangement. The CaM C-terminal lobe plugs the channel through a unique cation-π interaction by inserting the side chain of lysine K115 into a tetra-tryptophan cage at the ion channel pore intracellular entrance. Recent studies of TRPV6 structure and function described in this review advance our understanding of the role of this channel in physiology and pathophysiology and inform new therapeutic design.

Correspondence should be addressed to A.I.S. (as4005@cumc.columbia.edu).

Author contributions

M.V.Y., K.D.N., M.G.K. and A.I.S. drafted the manuscript and contributed figures and/or text to the manuscript and approved the final version. All authors agree to be accountable for all aspects of the work in ensuring that questions related to the accuracy or integrity of any part of the work are appropriately investigated and resolved and all persons designated as authors qualify for authorship, and all those who qualify for authorship are listed.

Additional information

Competing interests

The authors declare no competing interests.

Graphical Abstract

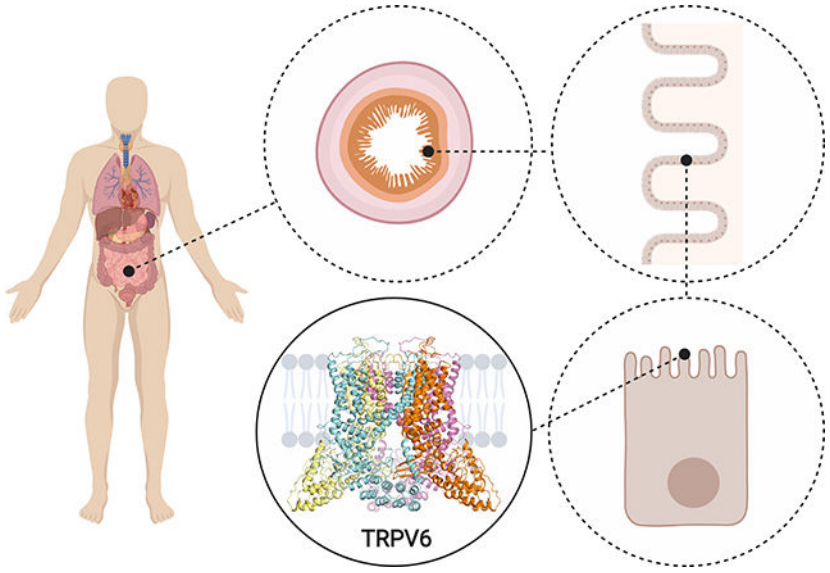

TRPV6 is a member of the TRPV (vanilloid) subfamily of the transient receptor potential (TRP) channel superfamily that is highly selective to Ca^{2+}. Apart from being the principal epithelial calcium channel for Ca^{2+} absorption in intestines and other organs, TRPV6 is important for bone development and male fertility. Mutations in TRPV6 are linked to hyperparathyroidism, while TRPV6 overexpression correlates with the development and progression of several human cancers. This review discusses recent advances in studies of TRPV6 using a combination of biophysical, biochemical and computational approaches, that have led to better understanding of structure and function of these channels and their role in physiology and disease.

Introduction

Calcium is the most abundant metal element in the human body. Of about 1 kg of calcium in the average adult, more than 99% is stored in the form of calcium phosphate as a critical component of bones and teeth (Brown, 1991; Peacock, 2010). The remaining ~10 g of calcium in the body is tightly regulated, of which about half exists in the free ionic Ca^{2+} form (Peacock, 2010; Robertson and Marshall, 1979). While the extracellular Ca^{2+} concentration is typically in the low millimolar range (~2 mM), the resting cell cytosolic Ca^{2+} is maintained at nearly 20,000-times lower concentration (~100 nM). Significant amounts of the intracellular calcium are stored inside organelles, such as mitochondria, endoplasmic and sarcoplasmic reticulum (Clapham, 2007). The steep Ca^{2+} concentration gradient and Ca^{2+} exchange between extracellular milieu and intracellular compartments are controlled with precision by various membrane ion channels and pumps as well as by cytosolic calcium-binding proteins. Such precise regulation allows Ca^{2+} to serve as a ubiquitous signaling molecule and regulate a plethora of physiological processes, including neurotransmitter release, muscle contraction, cell motility and gene expression (Clapham, 2007).

Human body's calcium homeostasis assumes three ways of increasing serum Ca^{2+} concentration (Peacock, 2010): (1) dietary intake and absorption by the intestine, (2) reabsorption by the kidney and (3) resorption from the bone. The first two processes occur in epithelial cells via paracellular and transcellular pathways (Hoenderop et al., 2005; Suzuki et al., 2008b) (Fig. 1a). In the paracellular pathway that is regulated by the claudin family transmembrane proteins, Ca^{2+} ions diffuse through intercellular tight junctions between the epithelial cells. The transcellular pathway includes three main steps (Hoenderop et al., 2005; Suzuki et al., 2008b): (1) absorption of luminal Ca^{2+} ions at the apical side of the epithelial cells, (2) transfer of Ca^{2+} ions to the basolateral membrane presumably by calbindin, whose role as a Ca^{2+} shuttle molecule is not unambiguous (Turnbull et al., 2004), and (3) extrusion of Ca^{2+} ions to the extracellular space via the ATP-dependent Ca^{2+}-ATPase PMCA1 and Na^{2+}/Ca^{2+} exchanger NCX1. The two molecules responsible for the step (1), apical Ca^{2+} entry, are calcium-selective channels TRPV5 and TRPV6 (Hoenderop et al., 1999; Peng et al., 1999). While TRPV5, which expression is mainly restricted to the kidney, is considered the major epithelial calcium channel for renal Ca^{2+} reabsorption, TRPV6 is considered the principal epithelial calcium channel for Ca^{2+} absorption in intestines and many other organs. Interestingly, in mice, TRPM7, rather than TRPV6, has been recently proposed to play the major role in intestinal Ca^{2+} absorption (Mittermeier et al., 2019), although in early development, TRPV6 contribution might still be critical (Beggs et al., 2019; Lee et al., 2019). In this review, we will focus on TRPV6.

TRPV6 (ECaC2 or CaT1) is a member of the TRPV (vanilloid) subfamily of the transient receptor potential (TRP) channel superfamily that is highly selective to Ca^{2+} ($P_{Ca}/P_{Na} > 100$) (den Dekker et al., 2003; Fecher-Trost et al., 2014; Hoenderop et al., 2001; Vennekens et al., 2002). Initially cloned from the duodenum (Peng et al., 1999), where it is highly concentrated at the microvilli tips of the lumen-facing epithelial cells (Fig. 1b), TRPV6 was also detected in other tissues showing expression in pancreas, prostate, salivary gland, sweat gland, liver, stomach, esophagus, kidney, placenta, testis, bone and blood cells (Giusti et al., 2014; Hirnet et al., 2003; Peng et al., 2000; Semenova et al., 2009). Expression of TRPV6 is regulated by the calcitropic hormone −1,25-dihydroxyvitamin D_3 ($1,25[OH]_2D_3$) (Balesaria et al., 2009; Meyer et al., 2006; Pike et al., 2007; Song et al., 2003), as the TRPV6 gene promoter has multiple vitamin-responsive elements, and also by dihydrotestosterone and estrogen (Peng et al., 2018; Song et al., 2003; Van Cromphaut et al., 2003). Important for Ca^{2+} absorption, TRPV6 channels have high calcium permeability, which distinguishes them and TRPV5 channels from other members of the TRP superfamily of cation channels (Hoenderop et al., 2002; Nijenhuis et al., 2003).

In cellular membranes, the cation-selective TRPV6 channels are constitutively active (den Dekker et al., 2003; Peng et al., 1999). However, single channel recordings from purified TRPV6 channels reconstituted into lipid bilayers (Zakharian et al., 2011) required phosphatidylinositol 4,5-bisphosphate (PIP_2), revealing an important role of lipids in regulation of channel activity. In the absence of extracellular Ca^{2+}, Na^+ can easily permeate through TRPV6 (Peng et al., 1999). High Ca^{2+} permeation can be documented by monitoring Ca^{2+} influx, for example, by loading cells with Ca^{2+} indicator (Fura-2) and performing ratiometric fluorescence measurements (Fig. 1c–d). Apart from Ca^{2+}, TRPV6 channels also conduct divalent cations Ba^{2+}, Sr^{2+} and Mn^{2+}, but not Mg^{2+} (Owsianik et al.,

2006; Peng et al., 1999). In fact, both extracellular and intracellular Mg^{2+} ions inhibit TRPV6 currents (Owsianik et al., 2006). Moreover, block by intracellular Mg^{2+} is partially responsible for the strong inward rectification displayed by these channels (Voets et al., 2003) (Fig. 1e). In addition, at low Mg^{2+} concentration, channels reconstituted in planar lipid bilayers showed inward currents that had larger conductance (~50 pS) and higher channel open probability (~0.93) than outward currents (~30 pS, open probability of ~0.28), indicating that the inward rectification of TRPV6 is also to a certain extent intrinsic and not reliant on cellular factors (Zakharian et al., 2011). A number of other divalent cations, Cu^{2+}, Pb^{2+}, and Cd^{2+}, trivalent cations La^{3+} and Gd^{3+} as well as protons produce marked TRPV6 inhibition (Hoenderop et al., 1999; Peng et al., 1999). There are several small-molecule inhibitors of TRPV6, including ruthenium red (Hoenderop et al., 2001; Vassilieva et al., 2013), 2-aminoethoxydiphenyl borate (Kovacs et al., 2012; Voets et al., 2001) and phytocannabinoid Δ9-tetrahydrocannabivarin (Janssens et al., 2018). TRPV6 channels are inactivated by intracellular Ca^{2+}. Several studies showed importance of calmodulin (CaM) for Ca^{2+}-dependent inactivation (Derler et al., 2006; Lambers et al., 2004; Nilius et al., 2002), with as many as seven CaM binding sites proposed based on sequence analysis (Bate et al., 2018; Cao et al., 2013a; Kovalevskaya et al., 2012).

Physiological roles of TRPV6 are not limited to intestinal Ca^{2+} absorption (Bianco et al., 2007). Unlike *Trpv5*$^{-/-}$ null mice, which exhibited a defect in bone formation due to excessive loss of Ca^{2+} in the urine (Hoenderop et al., 2003), *Trpv6*$^{-/-}$ null mice are still viable on a normal calcium diet (Weissgerber et al., 2012). However, *Trpv6*$^{-/-}$ null mice exhibit severely impaired male fertility accompanied by reduced motility and viability of sperm compared to the wild-type animals; they also show a significant increase in the epididymal luminal Ca^{2+} concentration that is mirrored by a lack of Ca^{2+} uptake by the epididymal epithelium (Weissgerber et al., 2012). In addition, knockout TRPV6$^{-/-}$ mice exhibit disordered Ca^{2+} homeostasis, including defective intestinal Ca^{2+} absorption, increased urinary Ca^{2+} excretion, decreased femoral bone mineral density, lower body weight, and 80% of the mice develop alopecia and dermatitis (Bianco et al., 2007; Lieben et al., 2010; Suzuki et al., 2008a; Weissgerber et al., 2012; Weissgerber et al., 2011). The TRPV6 mRNA and protein levels in placenta of women suffering from pre-eclampsia are decreased compared to healthy placental tissue (Hache et al., 2011). Several human TRPV6 gene mutations have been recently linked to transient neonatal hyperparathyroidism (Suzuki et al., 2018) as well as under-mineralization and dysplasia of the human skeleton (Burren et al., 2018), both phenotypes mirrored by a TRPV6 gene deletion in mice (Fecher-Trost et al., 2019). Changes in TRPV6 expression have also been shown in several other transgenic mouse models of human diseases, including Pendred syndrome (Wangemann et al., 2007), Crohn's-like disease (Huybers et al., 2008), Lowe syndrome and Dent disease (Wu et al., 2012), Gitelman syndrome (Yang et al., 2010) and kidney stone disease (Frick et al., 2013).

From the very early studies of TRPV6, it became apparent that TRPV6 transcripts are overexpressed in cancerous tissues and their derived cell lines; such increased expression stimulates the metastasis of cancer cells and confers chemotherapy resistance. It appears that the central role of TRPV6 in cancer is to impair Ca^{2+} homeostasis by stimulating Ca^{2+} entry into the cell or altering membrane potential. As shown by different methods, including Northern blot analysis, in situ hybridization and mass spectrometry, TRPV6 is overexpressed

in various types of human cancer cells, including breast, prostate, colon, ovarian, thyroid, endometrial and leukemia cancer cells (Bodding et al., 2003; Bolanz et al., 2008; Bolanz et al., 2009; Bowen et al., 2013; Fecher-Trost et al., 2014; Fixemer et al., 2003; Fleet et al., 2002; Lehen'kyi et al., 2011; Peng et al., 2000; Semenova et al., 2009; Taparia et al., 2006; Wissenbach et al., 2004; Wissenbach and Niemeyer, 2007; Wissenbach et al., 2001; Zheng et al., 2012; Zhuang et al., 2002). In case of breast cancer, it has been shown by microarray analysis, that overexpression of TRPV6, associated with reduced patient overall survival, is a feature of estrogen receptor-negative breast tumors as well as HER2-positive tumors. It was shown using TRPV6-transfected *Xenopus* oocytes, that tamoxifen, the most common therapy used in breast cancer treatment, inhibits the Ca^{2+} uptake mediated by TRPV6. Thus, TRPV6 is implicated in tumor development and progression and its overexpression pattern correlates with the aggressiveness of the disease (Fixemer et al., 2003; Lehen'kyi et al., 2007; Lehen'kyi et al., 2011; Lehen'kyi et al., 2012; Peng et al., 2001; Wissenbach et al., 2004; Wissenbach et al., 2001). Monitoring TRPV6 overexpression is therefore an effective way of early cancer detection.

TRPV6 expression was monitored using high-affinity peptide antagonists of human TRPV6 derived from the paralytic venom of the northern-tailed shrew (*Blarina brevicauda*) conjugated with a fluorescent dye or a magnetic resonance imaging (MRI) contrast agent as diagnostic tools to target tumor sites in mice bearing ovarian or prostate tumors (Bowen et al., 2013). Since Ca^{2+} is a critical regulator of cell proliferation, the link between tumor progression and TRPV6 overexpression also suggests an active role of calcium-permeable TRPV6 in the potentiation of calcium-dependent cell proliferation and inhibition of apoptosis (Bowen et al., 2013). For instance, epidemiologic studies have linked calcium-rich diets to a higher risk of prostate cancer (Chan and Giovannucci, 2001; Clinton and Giovannucci, 1998; Tavani et al., 2001). Inhibitors of TRPV6 may therefore offer a novel therapeutic strategy for treatment of TRPV6-rich tumors (Bolanz et al., 2008; Bowen et al., 2013; Lehen'kyi et al., 2007; Schwarz et al., 2006). For example, currently in clinical trials is the Soricimed C-series of peptides, which initiate apoptosis in human tumor xenografts and shrink tumors, while exhibiting a very low toxicity profile (Fu et al., 2017; Xue et al., 2018). In addition, development of selective small molecule inhibitors or channel blockers of TRPV6 has identified promising lead compounds for cancer treatment (Haverstick et al., 2000; Hofer et al., 2013; Kovacs et al., 2012; Landowski et al., 2011; Simonin et al., 2015). Since TRPV6 has proven to be an attractive drug target, it is important to better understand its molecular structure and function.

In this review, we discuss recent advances in studies of TRPV6 structure and function using a combination of biophysical, biochemical and computational methods, including structural and molecular biology, functional essays and molecular modeling, that have led to better understanding of the molecular bases of TRPV6 channels function and their role in physiology and disease.

Structural architecture

Four identical subunits, which are 725 residue-long in human TRPV6 (hTRPV6), assemble into a 4-fold symmetrical tetramer that includes two main compartments: a transmembrane

(TM) domain with a central ion channel pore and a ~70-Å tall and ~110 Å wide intracellular skirt where four subunits comprise walls enclosing a ~50 Å X 50 Å wide cavity underneath the ion channel (Fig. 2a–b). A single TRPV6 subunit contains an N-terminal helix, followed by an ankyrin repeat domain (ARD) with six ankyrin repeats, and a linker domain that includes a β hairpin (composed of β-strands β1 and β2) and a helix-turn-helix motif resembling a seventh ankyrin repeat, and the pre-S1 helix, which connects the linker domain to the TM domain (Fig. 2c–d). The TM domain of TRPV6 crudely resembles voltage gated K^+ (Long et al., 2007) or Na^+ (Payandeh et al., 2011) channels and includes six TM helices (S1-S6) and a pore loop (P-loop) between S5 and S6. The first four TM helices form a bundle to comprise the S1-S4 domain. In voltage-gated ion channels, the S1-S4 domain plays the role of a voltage sensor, in which the positively charged arginine and lysine residues of S4 move relative to the membrane plane during activation and deactivation of these channels. In TRPV6, S4 does not contain positively charged residues. Instead, extensive hydrophobic interactions between aromatic side chains in S1-S4 rigidifies the helical bundle conformation, suggesting that this domain remains relatively static during gating. Following S6 is the amphipathic TRP helix, which runs parallel to the membrane and creates a hub for interactions between hydrophobic elements of the TM domain and hydrophilic elements of the intracellular skirt.

Following the amphipathic TRP helix, the polypeptide forms a loop structure named C-terminal hook, which continues with a six-residue β-strand (β3) that tethers to the β hairpin in the linker domain to create a three-stranded β-sheet. The latter, together with the N-terminal helix and C-terminal hook, participate in intersubunit interactions with the ARDs that glue the elements of the intracellular skirt together. At the center of these interactions is the N-terminal helix, which is positioned as a pillar along the corners of the intracellular skirt. Deletions of the N-terminal helix or mutations of its conserved residues in the homologous TRPV5 abolished or significantly impaired its Ca^{2+} uptake function (de Groot et al., 2011b), suggesting that the intersubunit interactions are both structurally and functionally important.

On the extracellular side of the membrane, the intersubunit interactions are mediated by the S1-S2 extracellular loops contacting the S5-P and P-S6 loops of the adjacent subunit. Modification of a conserved N-linked glycosylation site in the S1-S2 loop is a likely reason for activation of TRPV5 and TRPV6 by the beta glucuronidase klotho (Lu et al., 2008). In the TM domain, the pore module elements S5, P-loop and S6 of the neighboring subunits are involved in extensive intersubunit interfaces to form the central ion channel pore. In addition, the pore-forming elements of each TRPV6 subunit interact extensively with the S1 and S4 helices of the adjacent subunit S1-S4 domain. The pore and S1-S4 domains therefore interact with each other in a domain-swapped arrangement (Fig. 2b), similar to other TRP channels (Chen et al., 2017; Guo et al., 2017; Hirschi et al., 2017; Jin et al., 2017; Liao et al., 2013; McGoldrick et al., 2019; Paulsen et al., 2015; Schmiege et al., 2017; Shen et al., 2016; Su et al., 2018; Tang et al., 2018; Winkler et al., 2017; Yin et al., 2018; Zhou et al., 2017) and classical voltage-gated potassium (Long et al., 2005), sodium (Shen et al., 2017) and calcium ion channels (Wu et al., 2015), but different from a non-swapped arrangement in CNG channels (Li et al., 2017), HCN channels (Lee and MacKinnon, 2017) and potassium channels Eag1 (Whicher and MacKinnon, 2016), Slo1 (Tao et al., 2017) and Slo2.2 (Hite

and MacKinnon, 2017). Interestingly, the non-swapped arrangement was observed in the first crystal structure of rat TRPV6 (rTRPV6) construct $TRPV6_{cryst}$ that had a single residue mutation L495Q in the TM domain and showed function, which was nearly identical to wild type channels (Saotome et al., 2016). Reversal of glutamine to the naturally occurring leucine in the new construct TRPV6* resulted in a remarkable change of the TRPV6 architecture to the domain-swapped arrangement (Singh et al., 2017). It turned out that the domain-swapped arrangement can also be reversed to the non-swapped arrangement by deletions in the S4-S5 linker connecting the pore and the S1-S4 domains (Singh et al., 2017), which was predicted to happen in the course of evolution in CNG, HCN, Eag1, Slo1 and Slo2.2 channels (Hite and MacKinnon, 2017; Lee and MacKinnon, 2017; Li et al., 2017; Tao et al., 2017; Whicher and MacKinnon, 2016). Shortening of the S4-S5 linker in TRPV6*, however, ablated channel-mediated calcium influx, suggesting that different types of the domain arrangement-switching mutations can lead to strong or weak changes in the ion channel function (Singh et al., 2017). It remains to be seen whether the domain arrangement-switching mutations are relevant to pathophysiology and disease and whether such an incredible switch in the domain architecture can happen in other ion channels.

Ion-conducting pore and cation binding sites

Architecture of the TRPV6 ion-conducting pore is conserved across the family of tetrameric ion channels. The extracellular segment of the pore is formed by extracellular loops connecting the P-loop helix to S5 and S6, while the rest of the ion conduction pathway is formed by the S6 helices (Fig. 3 and 4a). The region connecting S5 and S6 contains eight acidic residues per protomer, four of which face the ion conduction pathway, creating a highly electronegative entry to the pore (Fig. 3a–b). Below this extracellular vestibule is a four-residue selectivity filter formed by the extended portions of the re-entrant P-loops (Figs 3c–g and 4a). The side chains of the highly conserved aspartates (D542 in hTRPV6 and D541 in rTRPV6), which have previously been identified as critical for Ca^{2+} selectivity, permeation, and voltage-dependent Mg^{2+} block (Owsianik et al., 2006; Voets et al., 2003), protrude toward the pore central axis to produce a minimum interatomic distance of 4.6 Å at the upper tip of the selectivity filter, consistent with the pore diameter of 5.4 Å estimated based on the permeability of the channel to organic cations (Voets et al., 2004).

Below the selectivity filter, the pore widens into a large, mainly hydrophobic cavity. Lateral pore portals (Fig. 3a) may provide hydrophobic access to this cavity for small molecules or lipids, similar to voltage gated Na^{+} channels (Payandeh et al., 2011). The large diameter of the hydrophobic cavity (~13 Å) can easily accommodate a fully hydrated calcium ion, which has an effective diameter of 8–10 Å. The S6 helices cross at the intracellular portion of the channel. Conserved methionine (M578 in hTRPV6 and M577 in rTRPV6) side chains form a ~5 Å in diameter narrow constriction creating a hydrophobic seal and defining the lower gate (Fig. 4a), similar to TRPV2 (Zubcevic et al., 2016), TRPV3 (Singh et al., 2018a; Zubcevic et al., 2018), TRPV4 (Deng et al., 2018) and TRPV5 (Hughes et al., 2018a). Anomalous diffraction from the closed-state rTRPV6 crystals grown with selenomethionine-labeled protein strongly confirmed that M577 side chains occlude the pore (Saotome et al., 2016; Singh et al., 2017). Interestingly, despite high sequence conservation in this region, the equivalent methionine residue in the published non-conducting conformations of TRPV1

points away from the pore axis (Liao et al., 2013). Whether these structures represent intermediate rather than truly closed conformations of TRPV1 (see below) remains to be determined.

Binding of cations in the TRPV6 pore was studied by co-crystallizing $TRPV6_{cryst}$ with Ca^{2+}, Ba^{2+} or Gd^{3+}, which have various permeation and channel-blocking properties (Kovacs et al., 2011), and collecting X-ray diffraction data to locate anomalous difference peaks specific to each cation. The anomalous difference peaks suggest the presence of four types of cation binding sites in the $TRPV6_{cryst}$ channel pore (Fig. 3c–h). The main cation binding site (Site 1) is at the central pore axis at or near the same plane as D541 side chains. For Ca^{2+} ion at Site 1, the cation-oxygen distance of 2.4 Å (Fig. 4a) matches the reported average Ca^{2+}-oxygen distance calculated from crystal structures of various classes of Ca^{2+}-binding proteins (Yang et al., 2002). This minimal interatomic distance suggests that the carboxylate oxygens of D541 in rTRPV6 directly coordinate an at least partially dehydrated Ca^{2+} ion at this site. Similarly, structural studies of the hexameric Ca^{2+} release-activated channel Orai suggest that Ca^{2+} selectivity is achieved by direct coordination of Ca^{2+} by a ring of glutamate residues at the extracellular entrance to the pore (Hou et al., 2012). By contrast, in Ca_VAb, the permeant Ca^{2+} ion indirectly interacts with the pore through water molecules (Tang et al., 2014).

Another site (Site 2) located at the central pore axis of rTRPV6 was identified by anomalous difference signals for Ca^{2+} and Ba^{2+}; it is 6–8 Å below Site 1, between the backbone carbonyls and side chain hydroxyl groups of T538 (Figs 3c–f, 4a). The greater Ca^{2+}/Ba^{2+}-oxygen distance at Site 2 indicates that the cation is equatorially hydrated at this location. Although the chemical environment of Site 2 suggests that it binds cations at lower affinity than Site 1, the Ba^{2+} signal is stronger at this site. The different relative anomalous peak intensities at Sites 1 and 2 for Ca^{2+} and Ba^{2+}, as well as their slightly different positions at Site 1, may arise from the greater size of Ba^{2+} (~3 Å diameter) than Ca^{2+} (~2 Å diameter). This observation implies that the TRPV6 selectivity filter discriminates ions on the basis of size as well as charge.

The third site at the central pore axis of rTRPV6 was identified 6.8 Å below Site 2, in the center of the hydrophobic cavity, at the level of M569 (Figs 3c–f, 4a). The corresponding anomalous difference peaks were observed for both Ca^{2+} and Ba^{2+}, though for Ca^{2+}, the anomalous peak at Site 3 was less robust, presumably due to weaker anomalous diffraction properties. The signal at Site 3 suggests that cations bound here are ordered by water molecules, which can be held in place by weak hydrogen bonding interactions and pore helix dipoles pointing their partial negative charges toward the center of the hydrophobic cavity, similar to K^+ channels (Doyle et al., 1998).

Four symmetry-related cation binding sites were identified in the $TRPV6_{cryst}$ outer vestibule (recruitment sites). The corresponding anomalous difference peaks were observed for Ba^{2+} and Gd^{3+} in the vicinity of the negatively charged rTRPV6 residues D517, E518 and D547, but at distinct locations, probably due to difference in charge density. Although the anomalous difference peaks at the recruitment sites were not observed for Ca^{2+}, presumably due to lower affinity, reduced occupancy, or weaker anomalous signal, the highly

electronegative outer vestibule is likely involved in the general recruitment of cations toward the extracellular vestibule of the TRPV6 channel. Consistent with the results of isothermal titration calorimetry experiments for Gd^{3+} (Saotome et al., 2016), affinity of cations to the recruitment sites is probably lower than to Site 1.

Mechanism of ion permeation

The pore architecture and locations of cation binding sites in $TRPV6_{cryst}$ (Figs 3 and 4a) provided the first structural clues about ion permeation through TRPV6 and the calcium permeation mechanism in particular (Saotome et al., 2016). Close proximity of carboxylate side chains at Site 1 suggested that the absence of a bound Ca^{2+} ion would be energetically unfavorable due to charge repulsion between D541 side chains in rTRPV6. Thus, it is likely that a Ca^{2+} ion is, in effect, constitutively bound at Site 1 and removal of it from Site 1 would require immediate replacement with another Ca^{2+} ion, necessitating a “knock off” mechanism of permeation. Given the large energetic barrier of displacing Ca^{2+} ion at Site 1, a substantially high local concentration of Ca^{2+} would be necessary for permeation to proceed at physiological membrane voltages. Recruitment sites in the highly electronegative extracellular vestibule might serve this purpose.

Using $TRPV6_{cryst}$ structures as initial templates, the mechanism of TRPV6 ion permeation was studied in molecular dynamics (MD) simulations (Sakipov et al., 2018). First, equilibrium simulations predicted that Ca^{2+}, Ba^{2+} and Gd^{3+} ions occupied similar but not identical positions in the pore compared to Sites 1–3 identified in the crystal structures. For example, Ca^{2+} ion bound to Site 1 in the rTRPV6 crystal structure remained close to its original position (Site 1a), being coordinated by D541 and water from the extracellular vestibule, while the ion located at the crystal structure Site 2 shifted towards Site 1 (Site 1b), where it is coordinated by the D541 oxygen and the backbone oxygen of I539 in the selectivity filter along with water molecules. MD simulations therefore predicted that the crystallographically identified Site 1 is occupied by two Ca^{2+} ions, the result further supported by quantum mechanical energy calculations (Sakipov et al., 2018). Accordingly, the anomalous difference peak at the crystallographically identified Site 1 is likely a result of averaging over the two closely spaced positions 1a and 1b seen in MD simulations. Position of the third Ca^{2+} ion in the rTRPV6 pore, which was fairly mobile during simulation, fluctuated between Sites 2 and 3, being coordinated by T538 at Site 2 or water in the central cavity (Site 3). All ions located at the recruitment sites were also very mobile compared to ions at Sites 1a and 1b but during equilibrium simulations, they remained in close proximity to their original positions. The large hydrophobic cavity in the center of the channel was fully hydrated in these simulations, demonstrating that a fully solvated ion may pass the cavity with minimal energetic penalty.

Non-equilibrium simulations shed light on the dynamics of permeation through the selectivity filter, revealing several interesting findings. First, simulations showed that in the presence of ions no water binds to or crosses the pore constriction. Second, the modelled relative contribution of ions to TRPV6-mediated currents is consistent with the one originally predicted for calcium channels in physiological experiments (Almers and McCleskey, 1984; Heinemann et al., 1992; Hess and Tsien, 1984; Hoenderop et al., 2001;

Vennekens et al., 2001). Indeed, at low Ca^{2+} concentrations, the inward current through the TRPV6 channel is mainly carried by Na^{+} ions. At high Ca^{2+} concentrations, Ca^{2+} current prevails, making the channel highly selective to calcium. Ca^{2+} permeation follows the knock-off mechanism, that can be described as a two-stage process (Fig. 4b–f): (1) the pair of resident Ca^{2+} ions at Sites 1a and 1b (Fig. 4b) is approached by a Ca^{2+} ion from the recruitment sites (Fig. 4c), and (2) the resident Ca^{2+} ion from Site 1b departs to the central cavity (Fig. 4d). In this mechanism of permeation, there is a transition state that is characterized by three Ca^{2+} ions occupying two binding sites (Sites 1a and 1b) formed by D541 residues in rTRPV6. The life time of this transition state is determined by the wait time for a consorted fluctuation at two ion positions: the incoming ion motion towards the binding site and the lower resident ion motion towards the central cavity. In the case of Ca^{2+}, the transition state is a short-living state that is often hard to observe.

Apart from Ca^{2+}, TRPV6 is permeable to other divalent cations, with the ion permeation sequence $Ca^{2+} > Ba^{2+} \geq Sr^{2+} > Mn^{2+}$ (den Dekker et al., 2003; Hoenderop et al., 2005), and weakly permeable to trivalent cations, such as La^{3+} and Gd^{3+} (Kovacs et al., 2011). According to the MD simulations, both Ca^{2+} and Ba^{2+} ions permeate TRPV6 via the knock-off mechanism but the observed transition state that includes three ions at Site 1 in both cases has a remarkably different life time. Compared to the short-living transition state for Ca^{2+}, the transition state for Ba^{2+} is long-living and slows down the entire dynamics of permeation. The main difference between Ca^{2+} and Ba^{2+} comes from their different short-range interactions (van der Waals parameters) with the atoms in their first solvation shell: while Ba^{2+} has a larger radius, it also has a nearly three times stronger short-range attraction to nearby atoms, therefore residing at the binding site for longer time. For trivalent cations, MD simulations showed stable configurations of one Gd^{3+} ion bound at Site 1 at low concentrations of Gd^{3+} and two Gd^{3+} ions bound at Site 1 at high Gd^{3+} concentrations. In either condition, however, the pore was blocked for permeation by Gd^{3+}, with no water or counter ion permeation observed. Apparently, trivalent cations block divalent cations from permeating by virtue of their strong positive charge, which results in higher affinity to Site 1. Most likely, Ca^{2+} and Mg^{2+} block monovalent currents (Owsianik et al., 2006) through an analogous mechanism. The mechanism of Na^{+} permeation is drastically different. While permeation of Ca^{2+} clearly follows the knock-off mechanism, Na^{+} permeation does not. Indeed, in the absence of Ca^{2+}, many Na^{+} ions occupy the selectivity filter, and the ones that leave it going intracellularly move independently of those that approach it from the extracellular space, therefore lacking the crucial condition of the Ca^{2+} permeation knock-off mechanism (Sakipov et al., 2018).

Lipids

Phosphoinositol lipids, phosphatidylinositol 4,5-bisphosphate (PIP_2) in particular, directly activate TRPV6 (Zakharian et al., 2011). PIP_2 also activates TRPV5 (Lee et al., 2005), a close homologue of TRPV6. While no discernible lipid densities were observed in the crystal structures of TRPV6 (Saotome et al., 2016; Singh et al., 2017), the cryo-EM reconstructions reveal numerous well-resolved non-protein densities around the TMD that likely represent lipids (McGoldrick et al., 2018; Singh et al., 2018b; Singh et al., 2018c) (Fig. 5). Similarly positioned densities in the structures of other TRP channels (Gao et al.,

2016) were modeled as molecules of lipids, including phosphatidylinositol (PI), phosphatidylcholine (PC), and phosphatidylethanolamine (PE). There are four strong lipid-like densities (1–4) per subunit of TRPV6, of which density 4 has a clear head-and-two-tails appearance. Fitting different lipid molecules into hTRPV6 density 4 (McGoldrick et al., 2018) suggests that the chemical environment around the lipid head group, including the negatively charged aspartate D525 and polar Y349, Y509, Q513 and Y524, supports binding of PE or PC rather than PIP_2. Densities 1–3 have sausage-like appearances and might represent a wider variety of lipid-like molecules, including cholesterol. In fact, cholesterol might play a role of TRPV6 activator alternative to PIP_2 as the activity of these channels is decreased by cholesterol sequestration with methyl-β-cyclodextrin (Kever et al., 2019). In physiological conditions, however, some of the densities 1–3 sites might also be occupied by PIP_2 (Velisetty et al., 2016; Zakharian et al., 2011). For example, positively charged R470 and K484 as well as polar T479, Q483 and Q596 around hTRPV6 density 2 create a permissive chemical environment for the head group of PIP_2. However, the poor fit of PIP_2 into density 2 (McGoldrick et al., 2018) suggests that in the published cryo-EM structures of TRPV6 it represents a different molecule. In this regard, two weaker lipid-like densities 5 and 6 (Fig. 5) might also be candidates to represent PIP_2. Indeed, in the apparently open state structure of TRPV5 determined in the presence of added PIP_2 (Hughes et al., 2018b), the density assigned to PIP_2 is in closest proximity to lipid-like densities 5 and 6 in TRPV6 but more peripheral relative to the channel. However, the putative PIP_2 density in TRPV5 is rather poor to allow unambiguous interpretation and mutations of residues around it produced rather weak effects on currents recorded from TRPV5-expressing oocytes before and after incubation with wortmannin, an inhibitor of PI4-kinases (Hughes et al., 2018b). In addition, no such putative PIP_2 density was observed in the other apparently open state structures of TRPV5 (Dang et al., 2019) or TRPV6 (McGoldrick et al., 2018), where the lipid-like densities 5 and 6 appear exactly the same as in the corresponding closed state structures, making them unlikely candidates to represent PIP_2. Therefore, the mechanism of PIP_2 action and the location of its binding site in TRPV6 have yet to be resolved. Nevertheless, lipids appear to be an important component of TRPV6 gating and regulation, as it becomes obvious from the following chapters.

Activation gating and channel opening

All crystal structures of rat TRPV6 were determined in the closed state (Saotome et al., 2016; Singh et al., 2017), where the M577 side chains formed a hydrophobic “seal” on the cytoplasmic side of the S6 helices, similar to the M578 side chains in mutant hTRPV6-R470E channels (Fig. 6a,d). Conversely, interatomic distances within the pore of the very first cryo-EM structure of wild type human TRPV6 confirmed that the channel pore is open (Fig. 6b,e). The hTRPV6 open pore surface is lined by the side chains of D542, T539, N572, I575, D580 and W583, as well as the backbone carbonyl oxygens of I540, I541 and G579. The narrowest part of the hTRPV6 upper pore, the selectivity filter, is formed by the D542 side chains, one from each subunit, which project towards the center of the pore (Fig. 6b,e) and, similar to D541 in rTRPV6, play an important role in Ca^{2+} permeation by directly coordinating dehydrated Ca^{2+} ions (Saotome et al., 2016). The narrowest part of the hTRPV6 lower pore (9.6-Å interatomic distance) is defined by the side chains of I575 at the

S6 bundle crossing (Fig. 6b). This part of the pore is comparable in size to the pore of open TRPV1 (9.3-Å interatomic distance, measured between side chains of I679) (Gao et al., 2016) and is wide-open for conductance of hydrated Na^+ or Ca^{2+} ions.

Structurally, wild type hTRPV6 can be converted from the open to closed state by introducing a single R470 mutation at the lipid density 2. Density 2 coincides with the vanilloid binding site in TRPV1, which accommodates agonists, such as resiniferatoxin and capsaicin, and antagonists, like capsazepine (Gao et al., 2016), but in the absence of ligands, is occupied by the lipid phosphatidylinositol favoring the closed pore conformation (Gao et al., 2016). Mutant hTRPV6-R470E channels are functional but show ~10 times slower calcium uptake compared to wild type channels, consistent with their less frequent openings (McGoldrick et al., 2018). Supporting the idea that the density 2 represents an activating lipid, its size in hTRPV6-R470E became smaller (Fig. 6g) than in hTRPV6 (Fig. 6h). Confirming different physical occupancy of density 2, the side chain of Q483 in hTRPV6-R470E has an altered conformation that would cause clashing with the lipid density in wild type hTRPV6 (Fig. 6g–h). Supporting the role of Q483 in lipid recognition, an hTRPV6-Q483A mutant, while being functional, demonstrated a ~5 times slower calcium uptake compared to wild type channels (McGoldrick et al., 2018). Interestingly, cryo-EM structure of wild type rTRPV6 captures the channel in the closed state, identical to crystal structures. Consistently, the lipid density 2 in the cryo-EM structure of rTRPV6 is much weaker than in hTRPV6, indicating either lower occupancy or greater mobility of the putative bound lipid. Because rTRPV6 and hTRPV6 were purified in similar conditions, have 89% overall sequence identity, and have identical amino acid compositions of their lipid 2 binding pockets, it remains a puzzle why one channel was closed and the other open. For example, some lipids within the membranes of the protein-expressing HEK cells may be important for opening of hTRPV6 but not rTRPV6. Different conformations of rTRPV6 and hTRPV6 might also reflect the ease with which these constitutively active channels rapidly transition between gating states, and that very subtle changes can push this equilibrium towards one state or the other. Such subtle changes, for instance, can originate from different interactions of membrane-mimicking environment (amphipols or nanodiscs) with S1-S3. These helices contain the largest number of membrane lipid-facing residues (69%), of which only 80% are identical between rTRPV6 and hTRPV6.

The principal structural changes during hTRPV6 opening occur in the pore-lining helix S6 and originate at A566, a residue highly conserved in TRPV5 and TRPV6 and located right below the selectivity filter (Fig. 6a–b). Confirming its important role in gating, substitution of A566 with threonine, the homologous residue conserved in TRPV1–4, greatly reduces the hTRPV6 current amplitude and slows down calcium uptake by ~30 times (McGoldrick et al., 2018). Upon opening, S6, which has an α-helical conformation in the closed state, undergoes a local transition to a π-helix. Compared to α-helices, which have i+4 and i residues connected by hydrogen bonds, π-helices are defined by repeated i+5 → i hydrogen bonding. Typically, these short secondary structure elements occur in ~15% of proteins and are flanked on both sides by α-helical segments, thus appearing as α-aneurisms or π-bulges in the middle of α-helices (Cooley et al., 2010). Concurrently with the α-to-π transition in the middle of S6, the lower part of S6, which forms the gate in the closed state, rotates by ~100° and bends away from the pore axis by ~11°. Importantly, these rearrangements not

only widen the pore for permeant ions but also change the set of residues that face the hTRPV6 pore axis (e.g., N572 and I575 in the open state compared to L574 and M578 in the closed state). Alanine A566, therefore, acts as a hinge to allow hTRPV6 gating at the S6 bundle crossing without changing the conformation of the selectivity filter (Fig. 6a–b). Correspondingly, the selectivity filter appears to play a crucial role in TRPV6 channel ion permeation rather than gating.

While many representatives of the TRP channel family have a π-bulge in the middle of S6 (Autzen et al., 2018; Cao et al., 2013b; Chen et al., 2017; Duan et al., 2019; Duan et al., 2018; Gao et al., 2016; Grieben et al., 2017; Guo et al., 2017; Hirschi et al., 2017; Hughes et al., 2018b; Jin et al., 2017; Liao et al., 2013; McGoldrick et al., 2018; Paulsen et al., 2015; Schmiege et al., 2017; Shen et al., 2016; Singh et al., 2018a; Singh et al., 2018b; Su et al., 2018; Vinayagam et al., 2018; Winkler et al., 2017; Zhang et al., 2018; Zhou et al., 2017), it is unclear how common is the α-to-π transition in S6 during gating. For many of the TRP channel subtypes, this uncertainty is due to limited availability of structures in different gating conformations. The α-to-π transition was first discovered experimentally in TRPV6 (McGoldrick et al., 2018) but hypothesized earlier based on comparison of TRPV1 structures, which had the π-bulge in the middle of S6 (Cao et al., 2013b; Liao et al., 2013), and the structure of TRPV2, which had the entire S6 α-helical (Zubcevic et al., 2016). More recently, the α-to-π transition in S6 during gating was also observed in structures of TRPV2 (Dosey et al., 2019; Pumroy et al., 2019; Zubcevic et al., 2016; Zubcevic et al., 2019b), TRPV3 (Singh et al., 2019; Singh et al., 2018a; Zubcevic et al., 2019a; Zubcevic et al., 2018) and TRPV5 (Dang et al., 2019; Hughes et al., 2018a; Hughes et al., 2018b). Despite MD simulations and bioinformatics analysis also predicted the α-to-π transition to occur in TRPV1 (Kasimova et al., 2018a; Kasimova et al., 2018b), all structures of this channel that have been published so far show the π-bulge in the middle S6, which maintains its secondary structure in different gating conformations. While it remains to be seen how common is the α-to-π transition in S6 during gating of TRP channels, it is clearly quite unique for the tetrameric ion channel family. Indeed, K^+ channels do have a gating hinge in their pore-forming inner helices (Jiang et al., 2002; Jiang et al., 2003). However, this hinge is formed by a glycine located one residue C-terminally compared to the gating hinge alanine in TRPV6 and permits bending of the inner helices by ~30° without an α-to-π transition. The glycine hinge, like the alanine hinge in TRPV6, allows gating of K^+ channels to occur at the inner helices bundle crossing without changing the selectivity filter. However, unlike TRPV6, the glycine gating hinge in K^+ channels does not introduce a ~100° rotation of the lower parts of the pore-forming helices and correspondingly does not change the residues lining the pore gate region. An alanine gating hinge is present in the pore-forming helices of ionotropic glutamate receptor (iGluR) family tetrameric ion channels (Twomey et al., 2017). However, this alanine gating hinge is located at the ion channel gate region. Correspondingly, bending the pore-forming helices at the iGluR alanine gating hinge directly alters the diameter of the pore in close proximity to the gate without an α-to-π transition. Therefore, the α-to-π transition during gating is a unique feature of TRP channels that might be specific to their exclusive physiological roles.

For the regions involved in gating, pore opening in hTRPV6 is accompanied by the formation of two electrostatic bonds per subunit (Fig. 6g–h). A salt bridge forms between

Q473 in the S4-S5 elbow and R589 in the TRP helix, and a hydrogen bond forms between D489 in the S5 helix and T581 in the S6 helix. Neither interaction is present in the closed-state structures of hTRPV6-R470E or rTRPV6 and the formation of the hydrogen bond (D489-T581 in hTRPV6-R460E or D488-T580 in rTRPV6) is prevented by the side chain of M577 or M576, respectively (Fig. 6g). The importance of the D489-T581 interaction for hTRPV6 opening is supported by the observation that a mutation equivalent to T581A reduces the excessive constitutive activity of an hTRPV6-G516S mutant (Hofmann et al., 2017). We speculate that formation of the electrostatic bonds compensates the energetic cost of the unfavorable α-to-π helical transition in S6 during channel opening. This structural solution therefore maintains the relative stabilities and similar energy levels of both gating states and supports the constitutive activity of TRPV6. Accordingly, the open and closed conformations of TRPV6 remain in a state of readily tunable equilibrium that can be shifted towards either state by different stimuli, including lipids (Velisetty et al., 2016; Zakharian et al., 2011).

Inhibition by 2-APB

A membrane-permeable compound 2-aminoethoxydiphenyl borate (2-APB), one of the few known small-molecule inhibitors of TRPV6, has been shown to attenuate tumor growth and invasiveness in human cancer cell lines in vitro (Nelson, 2018). 2-APB was initially characterized as an inhibitor of Ins(1,4,5)P3 receptor-induced Ca^{2+} release (Maruyama et al., 1997) but was later shown to modulate the functions of different ion channels, including calcium release-activated (CRAC) (Xu et al., 2016) and two-pore potassium (K2P) (Zhuo et al., 2015) channels. 2-APB modulation of TRP channels (Colton and Zhu, 2007) includes activation of TRPV1, TRPV2, TRPV3, TRPA1 and TRPM6 (Chung et al., 2004; Hinman et al., 2006; Hu et al., 2004; Li et al., 2006) and inhibition of TRPM2, TRPM7, TRPC3, TRPC6 and TRPC7 (Chokshi et al., 2012; Lievremont et al., 2005; Togashi et al., 2008). The promiscuousness of 2-APB makes it an important research tool to characterize physiological function and biophysical properties of ion channels. However, the lack of specificity requires precise knowledge about 2-APB interaction with a target channel in order to explore its potential as a lead compound for drug design.

Structures of TRPV6 (Singh et al., 2018c) identified 2-APB binding site in a pocket formed by the intracellular portions of the S1-S4 helices and the membrane-facing sides of the amphipathic TRP helices (Fig. 7a–b). This site was confirmed crystallographically by the anomalous difference signal for a bromine derivative of 2-APB (Fig. 7b) and by mutagenesis (Singh et al., 2018c). Mutations in the 2-APB binding pocket, however, did not weaken the inhibitory potency of 2-APB but either had a little effect, or resulted in a remarkable 8- to 50-fold increase in 2-APB potency compared to wild-type channels. This increase, rather than reduction of 2-APB potency caused by mutations in its binding pocket, pointed to competition between 2-APB and the surrounding TM domain lipids as a possible cause of channel inhibition. In fact, while the channel undergoes closure in the presence of 2-APB (Fig. 7c–d), there are clear changes in lipid-like densities near the 2-APB binding site (Fig. 7e–f).

2-APB directly competes with the lipid represented by density 1 (Fig. 7e–f). Therefore, when 2-APB binds, it wrings this lipid out. 2-APB binding to hTRPV6 is also accompanied by movement of F425 and P424 in S3 towards the S4-S5 linker. As a result, hydrophobic residues from the S2-S3 linker (I420), N-terminal portion of S3 (P424, F425, V427, L428), C-terminal portion of S4 (M466) and S4-S5 linker (I486, F487) in hTRPV6 come closer together to form a hydrophobic cluster at the base of lipid density 2. Formation of the hydrophobic cluster helps 2-APB to "squeeze out" the density 2 activating lipid away from the S4-S5 linker and TRP helix. The accompanying rearrangements of the TM helices in hTRPV6 eliminate the salt bridge between Q473 in the S4-S5 linker and R589 in the TRP helix, and the hydrogen bond between D489 in the S5 helix and T581 in the S6 helix. These interactions compensate for the unfavorable α-to-π helical transition in S6 that occurs during channel opening and their removal makes S6 α-helical and promotes channel closure.

It is likely that 2-APB similarly modulates the activity of other channels by manipulating their interactions with bound lipids, but that the functional outcome (activation, inhibition, or no effect) depends on the exact nature of the channel-lipid complex and whether the lipids have a positive or negative regulatory role in channel gating. For example, the lack of 2-APB modulation of TRPV4 and TRPV5 (Hu et al., 2004) might be due to tighter binding of the density 1 lipid and inability of 2-APB to displace it. Better structural knowledge about interactions of 2-APB with the ion channel protein and the surrounding it lipids will guide the design of small hydrophobic molecules that can alter channel function in a specific way, possibly leading to novel therapeutic strategies.

Inactivation by calmodulin

Ca^{2+}-induced inactivation is a common regulatory mechanism for different ion channel families, including voltage-gated potassium (Jow et al., 2004), sodium (Herzog et al., 2003), calcium (Lee et al., 1999; Qin et al., 1999; Zuhlke et al., 1999), cyclic-nucleotide gated (Chen and Yau, 1994), ryanodine (Gomez and Yamaguchi, 2014) and ionotropic glutamate receptor channels (Medina et al., 1996). The influx of calcium into the cell often initiates a negative feedback mechanism that inactivates Ca^{2+}-permeable ion channels to protect cells from calcium overload. In many cases, Ca^{2+}-induced inactivation directly employs the universal calcium sensor calmodulin (CaM) (Kovalevskaya et al., 2013). TRPV6, as well as its close relative TRPV5, undergoes Ca^{2+}-induced inactivation through direct interaction with CaM (Kovalevskaya et al., 2012; Lambers et al., 2004). This interaction was first visualized in cryo-EM structures of TRPV6 (Singh et al., 2018b) followed by structures of TRPV5 from two independent research groups (Dang et al., 2019; Hughes et al., 2018b), all illustrating the same inactivation mechanism.

Structures of both hTRPV6-CaM and rTRPV6-CaM complexes demonstrated that one TRPV6 tetramer binds one two-lobe CaM molecule (Fig. 8a–c). CaM docks into a ~50 Å × 50 Å cavity underneath the channel that is enclosed by a ~110 Å-wide intracellular skirt. The cavity is large enough for CaM to fit almost entirely and be hardly visible from the side (Fig. 8a). CaM adopts an unusual head-to-tail arrangement for its N- and C-terminal lobes (Fig. 8d), different from any published CaM structures bound to ion channel fragments (Singh et al., 2018b). The highly flexible region, which connects the N- and C-terminal

lobes (Barbato et al., 1992) and forms a linker helix in the canonical dumbbell conformation of CaM (Tidow and Nissen, 2013), folds into two helices (h4 and h5) connected by a loop.

TRPV6-CaM structures reveal several surface regions of TRPV6 that interact with the two lobes of CaM. In the center of the first region is lysine K115, which protrudes from a loop between helices h6 and h7 of the C-terminal lobe of CaM and contacts all four TRPV6 subunits by sticking its side chain into the intracellular orifice of the ion channel pore formed by four tryptophans (W582 in rTRPV6, W583 in hTRPV6), one from each TRPV6 subunit at the S6 bundle crossing (Fig. 8e). These tryptophans are highly conserved in TRPV6 and TRPV5 and trap the side chain of K115 by forming a tight square cage with 4.2 Å between the plane of each indole ring and the ε-amino group of K115. This tryptophan cage provides a unique environment for an atypically strong cation-π interaction between the π-system of four tryptophan indole rings and the positively charged ε-amino group of lysine and has not been observed in any protein structure before. The importance of W583 for CaM-dependent Ca^{2+}-induced inactivation was demonstrated in experiments with TRPV5 where the W583A mutation induced cell death due to increased calcium influx (van der Wijst et al., 2017). Mutations of W583 to leucine and alanine greatly reduced CaM-mediated inactivation of TRPV5 and converted the channel into the open state (Dang et al., 2019; Hughes et al., 2018b).

The other surface regions of TRPV6 that interact with the N- and C-terminal lobes of CaM are spread over all four TRPV6 subunits and collectively include the ankyrin repeats AR1–6, linker helices LH1–2 and proximal and distal portions of the C-terminus. These regions represent numerous spots on the TRPV6 amino acid primary sequence and explain why up to seven CaM binding sites on TRPV5/6 have been proposed previously (Bate et al., 2018; Bokhovchuk et al., 2018; Cao et al., 2013a; de Groot et al., 2011a; Hirnet et al., 2003; Holakovska et al., 2011; Kovalevskaya et al., 2012; Lambers et al., 2004; Niemeyer et al., 2001), also illustrating the eye-opening power of structural biology. Together all interfaces between TRPV6 and CaM cover a surface area of 3176 $Å^2$. Despite the large size of these interfaces, TRPV6-CaM interactions seem to be rather weak and allow mobility of CaM with respect to TRPV6. Supporting this conclusion, the density for CaM in both hTRPV6-CaM and rTRPV6-CaM structures is of lower resolution compared to the channel core (Singh et al., 2018b). An exception to the generally weaker density for CaM is the portion from which K115 projects and binds extremely tightly at the intracellular entrance to the channel pore.

The CaM-bound structures suggest the mechanism of Ca^{2+}-induced inactivation of TRPV6 and TRPV5 (Dang et al., 2019; Hughes et al., 2018b; Singh et al., 2018b). It has been previously shown that the C-terminal lobe of CaM has higher affinity to Ca^{2+} compared to its N-terminal lobe (James et al., 1995; Linse et al., 1991). Accordingly, under basal calcium levels, the C-terminal lobe of CaM might always be bound to Ca^{2+} and to the distal C-terminus of TRPV6 (Bate et al., 2018; Bokhovchuk et al., 2018). Only after the channel opens, allowing Ca^{2+} influx into the cell and increasing the local concentration of Ca^{2+}, can the N-terminal lobe of CaM saturate its Ca^{2+} binding sites and bind to and stabilize the proximal C-terminus of the channel. Fully Ca^{2+}-bound N- and C-terminal lobes of CaM can then adopt the unique head-to-tail arrangement and fit snugly into the cavity underneath the

channel, with the C-terminal lobe approaching the pore intracellular entrance and the side chain of K115 sticking into the tetra-tryptophan cage. While this model of Ca^{2+}-induced inactivation of TRPV6 and TRPV5 appear to be quite attractive, many details of the inactivation mechanism remain unclear. For example, what is exact role of Ca^{2+}, occupancy of CaM binding sites and how many CaMs are simultaneously bound to the channel subunits at each step of the inactivation mechanism? More biophysical, biochemical and structural experiments are necessary to better understand the inactivation process.

Conformational ensemble

Ca^{2+}-induced inactivation diversifies the conformational ensemble of TRPV6. Indeed, when the channel undergoes inactivation, it enters a conformational state distinct from the open and closed states (Fig. 9). Strikingly, however, the overall shape of TRPV6 does not change much between the closed, open and inactivated states (Fig. 9a). In fact, strong conformational changes are localized only to the channel core region (Fig. 9b–c), with the central ion conducting pathway showing different pore profiles (Fig. 6) and radii (Fig. 9d). Remarkably, despite these differences, the selectivity filter of the TRPV6 pore in the inactivated state is similar to that of the closed and open states (Fig. 9b), strongly supporting its exclusive role in ion permeation and Ca^{2+} selectivity (McGoldrick et al., 2018; Saotome et al., 2016). Indeed, a relatively static outer pore domain represents a key difference between Ca^{2+}-selective TRPV5/6 and other TRPV channels, which gate in response to various stimuli and thus display a higher degree of structural plasticity, including conformational changes in the selectivity filter (Cao et al., 2013b; Singh et al., 2018a). Three phenylalanine residues (F530, F533 and F536 in rTRPV6) in the pore helix, which are conserved in TRPV5–6, but only one of which is conserved in TRPV1–4, may restrict the selectivity filter dynamics.

In contrast to the selectivity filter, the pore profile at the ion channel gate region is distinct in all three, closed, open and inactivated, states of hTRPV6 (Figs 6, 9d). Here, the narrowest pore constriction in the inactivated state is similar in diameter to that in the closed state except that the constriction is formed more extracellularly by I575, instead of by M578 in the closed state. Due to the aliphatic nature of the isoleucine side chain, this narrow constriction creates a hydrophobic seal impermeable to cations. Permeation through the TRPV6-CaM pore is also prevented directly by CaM, which plugs the pore by inserting the side chain of K115 into the intracellular pore orifice. Accordingly, the tryptophans that form the cage surrounding K115 are getting pulled towards the center of the pore making the radius of the pore at its intracellular entrance smaller in the inactivated state than in the closed and open states (Figs 6, 9d).

As described above, the energetically unfavorable α-to-π transition in S6 during hTRPV6 channel opening is compensated by formation of the salt bridge between Q473 in the S4-S5 elbow and R589 in the TRP helix and the hydrogen bond between D489 in S5 and T581 in S6 (McGoldrick et al., 2018; Saotome et al., 2016). Compared to the closed state, the lower portion of S6 in the open state rotates by ~100°, exposing a different set of residues to the hTRPV6 pore, including M578 that serves as the activation gate (Fig. 10). In contrast, during inactivation, the S6 helices maintain the α-to-π transition, similar to the open state.

As a result, their lower portions do not rotate and so they expose the same residues to the pore as they do in the open state. Instead, the S6 helices tilt towards the center of the hTRPV6 pore at the alanine A566 gating hinge (Figs 6 and 9). Because of the pore constriction, I575, which lines the bottom of the central cavity in the open state, hydrophobically seals the pore, creating an inactivation gate. Interestingly, the D489-T581 hydrogen bond, which compensates the energetically unfavorable α-to-π transition in S6 upon hTRPV6 channel opening, is also present in the inactivated state. The tilting of the S6 helices that accompanies hTRPV6 inactivation does, however, break the Q473-R589 salt bridge (Fig. 10). An additional energy needed to compensate the unfavorable α-to-π helical transition in S6 in the inactivated state likely comes from the cation-π interaction between the tryptophan cage and K115, which functions as an inactivating plug.

Conclusions and outlook

Recent structural, functional and molecular modeling studies of TRPV6 have greatly advanced our understanding of the mechanisms of its high Ca^{2+} selectivity, ion and water permeation, channel gating, inhibition by 2-APB and CaM-mediated Ca^{2+}-dependent inactivation (Fig. 10). Nevertheless, many questions about TRPV6 structure and function remain unanswered, including kinetics and energetics of ion and water permeation through the entirety of the ion channel pore in the open state; location of PIP_2 binding sites and the role of phosphoinositols in the TRPV6 activation gating mechanism; energetics and cooperativity of subunits during gating transitions; detailed steps of the CaM-mediated inactivation mechanism. One of the important directions of TRPV6 research is discovery and characterization of potential druggable sites on TRPV6 that can be targeted with small molecules and/or antibodies. Combining structural biology methods with pharmacological, physiological, biophysical, computer modeling and bioinformatics approaches will further help to understand the role of TRPV6 in physiology and disease and to develop new therapeutic strategies targeting TRPV6.

Acknowledgments

Funding

M.G.K. is supported by the NIH (R01 NS083660, R01 GM128195) and NSF (1818213). A.I.S. is supported by the NIH (R01 CA206573, R01 NS083660, R01 NS107253), NSF (1818213) and the Irma T. Hirschl Career Scientist Award.

References

Almers W, and McCleskey EW (1984). Non-selective conductance in calcium channels of frog muscle: calcium selectivity in a single-file pore. J Physiol 353, 585–608. [PubMed: 6090646]

Autzen HE, Myasnikov AG, Campbell MG, Asarnow D, Julius D, and Cheng Y (2018). Structure of the human TRPM4 ion channel in a lipid nanodisc. Science 359, 228–232. [PubMed: 29217581]

Balesaria S, Sangha S, and Walters JR (2009). Human duodenum responses to vitamin D metabolites of TRPV6 and other genes involved in calcium absorption. Am J Physiol Gastrointest Liver Physiol 297, G1193–1197. [PubMed: 19779013]

Barbato G, Ikura M, Kay LE, Pastor RW, and Bax A (1992). Backbone dynamics of calmodulin studied by 15N relaxation using inverse detected two-dimensional NMR spectroscopy: the central helix is flexible. Biochemistry 31, 5269–5278. [PubMed: 1606151]

Bate N, Caves RE, Skinner SP, Goult BT, Basran J, Mitcheson JS, and Vuister GW (2018). A Novel Mechanism for Calmodulin-Dependent Inactivation of Transient Receptor Potential Vanilloid 6. Biochemistry 57, 2611–2622. [PubMed: 29505720]

Beggs MR, Lee JJ, Busch K, Raza A, Dimke H, Weissgerber P, Engel J, Flockerzi V, and Alexander RT (2019). TRPV6 and Cav1.3 Mediate Distal Small Intestine Calcium Absorption Before Weaning. Cell Mol Gastroenterol Hepatol 8, 625–642. [PubMed: 31398491]

Bianco SD, Peng JB, Takanaga H, Suzuki Y, Crescenzi A, Kos CH, Zhuang L, Freeman MR, Gouveia CH, Wu J, et al. (2007). Marked disturbance of calcium homeostasis in mice with targeted disruption of the Trpv6 calcium channel gene. J Bone Miner Res 22, 274–285. [PubMed: 17129178]

Bodding M, Fecher-Trost C, and Flockerzi V (2003). Store-operated Ca2+ current and TRPV6 channels in lymph node prostate cancer cells. J Biol Chem 278, 50872–50879. [PubMed: 14534305]

Bokhovchuk FM, Bate N, Kovalevskaya NV, Goult BT, Spronk C, and Vuister GW (2018). The Structural Basis of Calcium-Dependent Inactivation of the Transient Receptor Potential Vanilloid 5 Channel. Biochemistry 57, 2623–2635. [PubMed: 29584409]

Bolanz KA, Hediger MA, and Landowski CP (2008). The role of TRPV6 in breast carcinogenesis. Mol Cancer Ther 7, 271–279. [PubMed: 18245667]

Bolanz KA, Kovacs GG, Landowski CP, and Hediger MA (2009). Tamoxifen inhibits TRPV6 activity via estrogen receptor-independent pathways in TRPV6-expressing MCF-7 breast cancer cells. Mol Cancer Res 7, 2000–2010. [PubMed: 19996302]

Bowen CV, DeBay D, Ewart HS, Gallant P, Gormley S, Ilenchuk TT, Iqbal U, Lutes T, Martina M, Mealing G, et al. (2013). In vivo detection of human TRPV6-rich tumors with anti-cancer peptides derived from soricidin. PLoS One 8, e58866. [PubMed: 23554944]

Brown EM (1991). Extracellular Ca2+ sensing, regulation of parathyroid cell function, and role of Ca2+ and other ions as extracellular (first) messengers. Physiol Rev 71, 371–411. [PubMed: 2006218]

Burren CP, Caswell R, Castle B, Welch CR, Hilliard TN, Smithson SF, and Ellard S (2018). TRPV6 compound heterozygous variants result in impaired placental calcium transport and severe undermineralization and dysplasia of the fetal skeleton. Am J Med Genet A 176, 1950–1955. [PubMed: 30144375]

Cao C, Zakharian E, Borbiro I, and Rohacs T (2013a). Interplay between calmodulin and phosphatidylinositol 4,5-bisphosphate in Ca2+-induced inactivation of transient receptor potential vanilloid 6 channels. J Biol Chem 288, 5278–5290. [PubMed: 23300090]

Cao E, Liao M, Cheng Y, and Julius D (2013b). TRPV1 structures in distinct conformations reveal activation mechanisms. Nature 504, 113–118. [PubMed: 24305161]

Chan JM, and Giovannucci EL (2001). Dairy products, calcium, and vitamin D and risk of prostate cancer. Epidemiol Rev 23, 87–92. [PubMed: 11588859]

Chen Q, She J, Zeng W, Guo J, Xu H, Bai XC, and Jiang Y (2017). Structure of mammalian endolysosomal TRPML1 channel in nanodiscs. Nature 550, 415–418. [PubMed: 29019981]

Chen TY, and Yau KW (1994). Direct modulation by Ca(2+)-calmodulin of cyclic nucleotide-activated channel of rat olfactory receptor neurons. Nature 368, 545–548. [PubMed: 7511217]

Chokshi R, Fruasaha P, and Kozak JA (2012). 2-aminoethyl diphenyl borinate (2-APB) inhibits TRPM7 channels through an intracellular acidification mechanism. Channels (Austin) 6, 362–369. [PubMed: 22922232]

Chung MK, Lee H, Mizuno A, Suzuki M, and Caterina MJ (2004). 2-aminoethoxydiphenyl borate activates and sensitizes the heat-gated ion channel TRPV3. J Neurosci 24, 5177–5182. [PubMed: 15175387]

Clapham DE (2007). Calcium signaling. Cell 131, 1047–1058. [PubMed: 18083096]

Clinton SK, and Giovannucci E (1998). Diet, nutrition, and prostate cancer. Annu Rev Nutr 18, 413–440. [PubMed: 9706231]

Colton CK, and Zhu MX (2007). 2-Aminoethoxydiphenyl borate as a common activator of TRPV1, TRPV2, and TRPV3 channels. Handb Exp Pharmacol, 173–187. [PubMed: 17217057]

Cooley RB, Arp DJ, and Karplus PA (2010). Evolutionary origin of a secondary structure: pi-helices as cryptic but widespread insertional variations of alpha-helices that enhance protein functionality. J Mol Biol 404, 232–246. [PubMed: 20888342]

Dang S, van Goor MK, Asarnow D, Wang Y, Julius D, Cheng Y, and van der Wijst J (2019). Structural insight into TRPV5 channel function and modulation. Proc Natl Acad Sci U S A 116, 8869–8878. [PubMed: 30975749]

de Groot T, Kovalevskaya NV, Verkaart S, Schilderink N, Felici M, van der Hagen EA, Bindels RJ, Vuister GW, and Hoenderop JG (2011a). Molecular mechanisms of calmodulin action on TRPV5 and modulation by parathyroid hormone. Mol Cell Biol 31, 2845–2853. [PubMed: 21576356]

de Groot T, van der Hagen EA, Verkaart S, te Boekhorst VA, Bindels RJ, and Hoenderop JG (2011b). Role of the transient receptor potential vanilloid 5 (TRPV5) protein N terminus in channel activity, tetramerization, and trafficking. J Biol Chem 286, 32132–32139. [PubMed: 21795703]

den Dekker E, Hoenderop JG, Nilius B, and Bindels RJ (2003). The epithelial calcium channels, TRPV5 & TRPV6: from identification towards regulation. Cell Calcium 33, 497–507. [PubMed: 12765695]

Deng Z, Paknejad N, Maksaev G, Sala-Rabanal M, Nichols CG, Hite RK, and Yuan P (2018). Cryo-EM and X-ray structures of TRPV4 reveal insight into ion permeation and gating mechanisms. Nat Struct Mol Biol 25, 252–260. [PubMed: 29483651]

Derler I, Hofbauer M, Kahr H, Fritsch R, Muik M, Kepplinger K, Hack ME, Moritz S, Schindl R, Groschner K, et al. (2006). Dynamic but not constitutive association of calmodulin with rat TRPV6 channels enables fine tuning of Ca2+-dependent inactivation. J Physiol 577, 31–44. [PubMed: 16959851]

Dosey TL, Wang Z, Fan G, Zhang Z, Serysheva II, Chiu W, and Wensel TG (2019). Structures of TRPV2 in distinct conformations provide insight into role of the pore turret. Nat Struct Mol Biol 26, 40–49. [PubMed: 30598551]

Doyle DA, Morais Cabral J, Pfuetzner RA, Kuo A, Gulbis JM, Cohen SL, Chait BT, and MacKinnon R (1998). The structure of the potassium channel: molecular basis of K+ conduction and selectivity. Science 280, 69–77. [PubMed: 9525859]

Duan J, Li J, Chen GL, Ge Y, Liu J, Xie K, Peng X, Zhou W, Zhong J, Zhang Y, et al. (2019). Cryo-EM structure of TRPC5 at 2.8-A resolution reveals unique and conserved structural elements essential for channel function. Sci Adv 5, eaaw7935. [PubMed: 31355338]

Duan J, Li Z, Li J, Hulse RE, Santa-Cruz A, Valinsky WC, Abiria SA, Krapivinsky G, Zhang J, and Clapham DE (2018). Structure of the mammalian TRPM7, a magnesium channel required during embryonic development. Proc Natl Acad Sci U S A 115, E8201–E8210. [PubMed: 30108148]

Fecher-Trost C, Lux F, Busch KM, Raza A, Winter M, Hielscher F, Belkacemi T, van der Eerden B, Boehm U, Freichel M, et al. (2019). Maternal Transient Receptor Potential Vanilloid 6 (Trpv6) Is Involved In Offspring Bone Development. J Bone Miner Res 34, 699–710. [PubMed: 30786075]

Fecher-Trost C, Weissgerber P, and Wissenbach U (2014). TRPV6 channels. Handb Exp Pharmacol 222, 359–384. [PubMed: 24756713]

Fixemer T, Wissenbach U, Flockerzi V, and Bonkhoff H (2003). Expression of the Ca2+-selective cation channel TRPV6 in human prostate cancer: a novel prognostic marker for tumor progression. Oncogene 22, 7858–7861. [PubMed: 14586412]

Fleet JC, Eksir F, Hance KW, and Wood RJ (2002). Vitamin D-inducible calcium transport and gene expression in three Caco-2 cell lines. Am J Physiol Gastrointest Liver Physiol 283, G618–625. [PubMed: 12181175]

Frick KK, Asplin JR, Favus MJ, Culbertson C, Krieger NS, and Bushinsky DA (2013). Increased biological response to 1,25(OH)(2)D(3) in genetic hypercalciuric stone-forming rats. Am J Physiol Renal Physiol 304, F718–726. [PubMed: 23344574]

Fu S, Hirte H, Welch S, Ilenchuk TT, Lutes T, Rice C, Fields N, Nemet A, Dugourd D, Piha-Paul S, et al. (2017). First-in-human phase I study of SOR-C13, a TRPV6 calcium channel inhibitor, in patients with advanced solid tumors. Invest New Drugs 35, 324–333. [PubMed: 28150073]

Gao Y, Cao E, Julius D, and Cheng Y (2016). TRPV1 structures in nanodiscs reveal mechanisms of ligand and lipid action. Nature 534, 347–351. [PubMed: 27281200]

Giusti L, Cetani F, Da Valle Y, Pardi E, Ciregia F, Donadio E, Gargini C, Piano I, Borsari S, Jaber A, et al. (2014). First evidence of TRPV5 and TRPV6 channels in human parathyroid glands: possible involvement in neoplastic transformation. J Cell Mol Med 18, 1944–1952. [PubMed: 25164318]

Gomez AC, and Yamaguchi N (2014). Two regions of the ryanodine receptor calcium channel are involved in Ca(2+)-dependent inactivation. Biochemistry 53, 1373–1379. [PubMed: 24521037]

Grieben M, Pike AC, Shintre CA, Venturi E, El-Ajouz S, Tessitore A, Shrestha L, Mukhopadhyay S, Mahajan P, Chalk R, et al. (2017). Structure of the polycystic kidney disease TRP channel Polycystin-2 (PC2). Nat Struct Mol Biol 24, 114–122. [PubMed: 27991905]

Guo J, She J, Zeng W, Chen Q, Bai XC, and Jiang Y (2017). Structures of the calcium-activated, non-selective cation channel TRPM4. Nature 552, 205–209. [PubMed: 29211714]

Hache S, Takser L, LeBellego F, Weiler H, Leduc L, Forest JC, Giguere Y, Masse A, Barbeau B, and Lafond J (2011). Alteration of calcium homeostasis in primary preeclamptic syncytiotrophoblasts: effect on calcium exchange in placenta. J Cell Mol Med 15, 654–667. [PubMed: 20178461]

Haverstick DM, Heady TN, Macdonald TL, and Gray LS (2000). Inhibition of human prostate cancer proliferation in vitro and in a mouse model by a compound synthesized to block Ca2+ entry. Cancer Res 60, 1002–1008. [PubMed: 10706116]

Heinemann SH, Terlau H, Stuhmer W, Imoto K, and Numa S (1992). Calcium channel characteristics conferred on the sodium channel by single mutations. Nature 356, 441–443. [PubMed: 1313551]

Herzog RI, Liu C, Waxman SG, and Cummins TR (2003). Calmodulin binds to the C terminus of sodium channels Nav1.4 and Nav1.6 and differentially modulates their functional properties. J Neurosci 23, 8261–8270. [PubMed: 12967988]

Hess P, and Tsien RW (1984). Mechanism of ion permeation through calcium channels. Nature 309, 453–456. [PubMed: 6328315]

Hinman A, Chuang HH, Bautista DM, and Julius D (2006). TRP channel activation by reversible covalent modification. Proc Natl Acad Sci U S A 103, 19564–19568. [PubMed: 17164327]

Hirnet D, Olausson J, Fecher-Trost C, Bodding M, Nastainczyk W, Wissenbach U, Flockerzi V, and Freichel M (2003). The TRPV6 gene, cDNA and protein. Cell Calcium 33, 509–518. [PubMed: 12765696]

Hirschi M, Herzik MA Jr., Wie J, Suo Y, Borschel WF, Ren D, Lander GC, and Lee SY (2017). Cryo-electron microscopy structure of the lysosomal calcium-permeable channel TRPML3. Nature 550, 411–414. [PubMed: 29019979]

Hite RK, and MacKinnon R (2017). Structural Titration of Slo2.2, a Na(+)-Dependent K(+) Channel. Cell 168, 390–399 e311. [PubMed: 28111072]

Hoenderop JG, Nilius B, and Bindels RJ (2002). Molecular mechanism of active Ca2+ reabsorption in the distal nephron. Annu Rev Physiol 64, 529–549. [PubMed: 11826278]

Hoenderop JG, Nilius B, and Bindels RJ (2005). Calcium absorption across epithelia. Physiol Rev 85, 373–422. [PubMed: 15618484]

Hoenderop JG, van der Kemp AW, Hartog A, van de Graaf SF, van Os CH, Willems PH, and Bindels RJ (1999). Molecular identification of the apical Ca2+ channel in 1, 25-dihydroxyvitamin D3-responsive epithelia. J Biol Chem 274, 8375–8378. [PubMed: 10085067]

Hoenderop JG, van Leeuwen JP, van der Eerden BC, Kersten FF, van der Kemp AW, Merillat AM, Waarsing JH, Rossier BC, Vallon V, Hummler E, et al. (2003). Renal Ca2+ wasting, hyperabsorption, and reduced bone thickness in mice lacking TRPV5. J Clin Invest 112, 1906–1914. [PubMed: 14679186]

Hoenderop JG, Vennekens R, Muller D, Prenen J, Droogmans G, Bindels RJ, and Nilius B (2001). Function and expression of the epithelial Ca(2+) channel family: comparison of mammalian ECaC1 and 2. J Physiol 537, 747–761. [PubMed: 11744752]

Hofer A, Kovacs G, Zappatini A, Leuenberger M, Hediger MA, and Lochner M (2013). Design, synthesis and pharmacological characterization of analogs of 2-aminoethyl diphenylborinate (2-APB), a known store-operated calcium channel blocker, for inhibition of TRPV6-mediated calcium transport. Bioorg Med Chem 21, 3202–3213. [PubMed: 23602525]

Hofmann L, Wang H, Beck A, Wissenbach U, and Flockerzi V (2017). A conserved gating element in TRPV6 channels. Cell Calcium 63, 24–28. [PubMed: 28029385]

Holakovska B, Grycova L, Bily J, and Teisinger J (2011). Characterization of calmodulin binding domains in TRPV2 and TRPV5 C-tails. Amino Acids 40, 741–748. [PubMed: 20686800]

Hou X, Pedi L, Diver MM, and Long SB (2012). Crystal structure of the calcium release-activated calcium channel Orai. Science 338, 1308–1313. [PubMed: 23180775]

Hu HZ, Gu Q, Wang C, Colton CK, Tang J, Kinoshita-Kawada M, Lee LY, Wood JD, and Zhu MX (2004). 2-aminoethoxydiphenyl borate is a common activator of TRPV1, TRPV2, and TRPV3. J Biol Chem 279, 35741–35748. [PubMed: 15194687]

Hughes TET, Lodowski DT, Huynh KW, Yazici A, Del Rosario J, Kapoor A, Basak S, Samanta A, Han X, Chakrapani S, et al. (2018a). Structural basis of TRPV5 channel inhibition by econazole revealed by cryo-EM. Nat Struct Mol Biol 25, 53–60. [PubMed: 29323279]

Hughes TET, Pumroy RA, Yazici AT, Kasimova MA, Fluck EC, Huynh KW, Samanta A, Molugu SK, Zhou ZH, Carnevale V, et al. (2018b). Structural insights on TRPV5 gating by endogenous modulators. Nat Commun 9, 4198. [PubMed: 30305626]

Huybers S, Apostolaki M, van der Eerden BC, Kollias G, Naber TH, Bindels RJ, and Hoenderop JG (2008). Murine TNF(DeltaARE) Crohn's disease model displays diminished expression of intestinal Ca2+ transporters. Inflamm Bowel Dis 14, 803–811. [PubMed: 18266230]

James P, Vorherr T, and Carafoli E (1995). Calmodulin-binding domains: just two faced or multi-faceted? Trends Biochem Sci 20, 38–42. [PubMed: 7878743]

Janssens A, Silvestri C, Martella A, Vanoevelen JM, Di Marzo V, and Voets T (2018). Delta(9)-tetrahydrocannabivarin impairs epithelial calcium transport through inhibition of TRPV5 and TRPV6. Pharmacol Res 136, 83–89. [PubMed: 30170189]

Jiang Y, Lee A, Chen J, Cadene M, Chait BT, and MacKinnon R (2002). The open pore conformation of potassium channels. Nature 417, 523–526. [PubMed: 12037560]

Jiang Y, Lee A, Chen J, Ruta V, Cadene M, Chait BT, and MacKinnon R (2003). X-ray structure of a voltage-dependent K+ channel. Nature 423, 33–41. [PubMed: 12721618]

Jin P, Bulkley D, Guo Y, Zhang W, Guo Z, Huynh W, Wu S, Meltzer S, Cheng T, Jan LY, et al. (2017). Electron cryo-microscopy structure of the mechanotransduction channel NOMPC. Nature 547, 118–122. [PubMed: 28658211]

Jow F, Zhang ZH, Kopsco DC, Carroll KC, and Wang K (2004). Functional coupling of intracellular calcium and inactivation of voltage-gated Kv1.1/Kvbeta1.1 A-type K+ channels. Proc Natl Acad Sci U S A 101, 15535–15540. [PubMed: 15486093]

Kasimova MA, Yazici A, Yudin Y, Granata D, Klein ML, Rohacs T, and Carnevale V (2018a). Ion Channel Sensing: Are Fluctuations the Crux of the Matter? J Phys Chem Lett 9, 1260–1264. [PubMed: 29439562]

Kasimova MA, Yazici AT, Yudin Y, Granata D, Klein ML, Rohacs T, and Carnevale V (2018b). A hypothetical molecular mechanism for TRPV1 activation that invokes rotation of an S6 asparagine. J Gen Physiol 150, 1554–1566. [PubMed: 30333107]

Kever L, Cherezova A, Zenin V, Negulyaev Y, Komissarchik Y, and Semenova S (2019). Downregulation of TRPV6 channel activity by cholesterol depletion in Jurkat T cell line. Cell Biol Int 43, 965–975. [PubMed: 31141273]

Kovacs G, Danko T, Bergeron MJ, Balazs B, Suzuki Y, Zsembery A, and Hediger MA (2011). Heavy metal cations permeate the TRPV6 epithelial cation channel. Cell Calcium 49, 43–55. [PubMed: 21146870]

Kovacs G, Montalbetti N, Simonin A, Danko T, Balazs B, Zsembery A, and Hediger MA (2012). Inhibition of the human epithelial calcium channel TRPV6 by 2-aminoethoxydiphenyl borate (2-APB). Cell Calcium 52, 468–480. [PubMed: 23040501]

Kovalevskaya NV, Bokhovchuk FM, and Vuister GW (2012). The TRPV5/6 calcium channels contain multiple calmodulin binding sites with differential binding properties. J Struct Funct Genomics 13, 91–100. [PubMed: 22354706]

Kovalevskaya NV, van de Waterbeemd M, Bokhovchuk FM, Bate N, Bindels RJ, Hoenderop JG, and Vuister GW (2013). Structural analysis of calmodulin binding to ion channels demonstrates the role of its plasticity in regulation. Pflugers Arch 465, 1507–1519. [PubMed: 23609407]

Lambers TT, Weidema AF, Nilius B, Hoenderop JG, and Bindels RJ (2004). Regulation of the mouse epithelial Ca2(+) channel TRPV6 by the Ca(2+)-sensor calmodulin. J Biol Chem 279, 28855–28861. [PubMed: 15123711]

Landowski CP, Bolanz KA, Suzuki Y, and Hediger MA (2011). Chemical inhibitors of the calcium entry channel TRPV6. Pharm Res 28, 322–330. [PubMed: 21057859]

Lee A, Wong ST, Gallagher D, Li B, Storm DR, Scheuer T, and Catterall WA (1999). Ca2+/calmodulin binds to and modulates P/Q-type calcium channels. Nature 399, 155–159. [PubMed: 10335845]

Lee CH, and MacKinnon R (2017). Structures of the Human HCN1 Hyperpolarization-Activated Channel. Cell 168, 111–120 e111. [PubMed: 28086084]

Lee J, Cha SK, Sun TJ, and Huang CL (2005). PIP2 activates TRPV5 and releases its inhibition by intracellular Mg2+. J Gen Physiol 126, 439–451. [PubMed: 16230466]

Lee JJ, Liu X, O'Neill D, Beggs MR, Weissgerber P, Flockerzi V, Chen XZ, Dimke H, and Alexander RT (2019). Activation of the calcium sensing receptor attenuates TRPV6-dependent intestinal calcium absorption. JCI Insight 5.

Lehen'kyi V, Flourakis M, Skryma R, and Prevarskaya N (2007). TRPV6 channel controls prostate cancer cell proliferation via Ca(2+)/NFAT-dependent pathways. Oncogene 26, 7380–7385. [PubMed: 17533368]

Lehen'kyi V, Raphael M, Oulidi A, Flourakis M, Khalimonchyk S, Kondratskyi A, Gordienko DV, Mauroy B, Bonnal JL, Skryma R, et al. (2011). TRPV6 determines the effect of vitamin D3 on prostate cancer cell growth. PLoS One 6, e16856. [PubMed: 21347289]

Lehen'kyi V, Raphael M, and Prevarskaya N (2012). The role of the TRPV6 channel in cancer. J Physiol 590, 1369–1376. [PubMed: 22331416]

Li M, Jiang J, and Yue L (2006). Functional characterization of homo- and heteromeric channel kinases TRPM6 and TRPM7. J Gen Physiol 127, 525–537. [PubMed: 16636202]

Li M, Zhou X, Wang S, Michailidis I, Gong Y, Su D, Li H, Li X, and Yang J (2017). Structure of a eukaryotic cyclic-nucleotide-gated channel. Nature 542, 60–65. [PubMed: 28099415]

Liao M, Cao E, Julius D, and Cheng Y (2013). Structure of the TRPV1 ion channel determined by electron cryo-microscopy. Nature 504, 107–112. [PubMed: 24305160]

Lieben L, Benn BS, Ajibade D, Stockmans I, Moermans K, Hediger MA, Peng JB, Christakos S, Bouillon R, and Carmeliet G (2010). Trpv6 mediates intestinal calcium absorption during calcium restriction and contributes to bone homeostasis. Bone 47, 301–308. [PubMed: 20399919]

Lievremont JP, Bird GS, and Putney JW Jr. (2005). Mechanism of inhibition of TRPC cation channels by 2-aminoethoxydiphenylborane. Mol Pharmacol 68, 758–762. [PubMed: 15933213]

Linse S, Helmersson A, and Forsen S (1991). Calcium binding to calmodulin and its globular domains. J Biol Chem 266, 8050–8054. [PubMed: 1902469]

Long SB, Campbell EB, and Mackinnon R (2005). Crystal structure of a mammalian voltage-dependent Shaker family K+ channel. Science 309, 897–903. [PubMed: 16002581]

Long SB, Tao X, Campbell EB, and MacKinnon R (2007). Atomic structure of a voltage-dependent K + channel in a lipid membrane-like environment. Nature 450, 376–382. [PubMed: 18004376]

Lu P, Boros S, Chang Q, Bindels RJ, and Hoenderop JG (2008). The beta-glucuronidase klotho exclusively activates the epithelial Ca2+ channels TRPV5 and TRPV6. Nephrol Dial Transplant 23, 3397–3402. [PubMed: 18495742]

Maruyama T, Kanaji T, Nakade S, Kanno T, and Mikoshiba K (1997). 2APB, 2-aminoethoxydiphenyl borate, a membrane-penetrable modulator of Ins(1,4,5)P3-induced Ca2+ release. J Biochem 122, 498–505. [PubMed: 9348075]

McGoldrick LL, Singh AK, Demirkhanyan L, Lin TY, Casner RG, Zakharian E, and Sobolevsky AI (2019). Structure of the thermo-sensitive TRP channel TRP1 from the alga Chlamydomonas reinhardtii. Nat Commun 10, 4180. [PubMed: 31519888]

McGoldrick LL, Singh AK, Saotome K, Yelshanskaya MV, Twomey EC, Grassucci RA, and Sobolevsky AI (2018). Opening of the human epithelial calcium channel TRPV6. Nature 553, 233–237. [PubMed: 29258289]

Medina I, Filippova N, Bakhramov A, and Bregestovski P (1996). Calcium-induced inactivation of NMDA receptor-channels evolves independently of run-down in cultured rat brain neurones. J Physiol 495 (Pt 2), 411–427. [PubMed: 8887753]

Meyer MB, Watanuki M, Kim S, Shevde NK, and Pike JW (2006). The human transient receptor potential vanilloid type 6 distal promoter contains multiple vitamin D receptor binding sites that mediate activation by 1,25-dihydroxyvitamin D3 in intestinal cells. Mol Endocrinol 20, 1447–1461. [PubMed: 16574738]

Mittermeier L, Demirkhanyan L, Stadlbauer B, Breit A, Recordati C, Hilgendorff A, Matsushita M, Braun A, Simmons DG, Zakharian E, et al. (2019). TRPM7 is the central gatekeeper of intestinal mineral absorption essential for postnatal survival. Proc Natl Acad Sci U S A 116, 4706–4715. [PubMed: 30770447]

Nelson AM, Moayedi Y, Greenberg SA, Ruiz ME, Jensen UB, Owens DM, and Lumpkin EA (2018). 2-APB arrests human keratinocyte proliferation and inhibits cutaneous squamous cell carcinoma in vitro. bioRxiv.

Niemeyer BA, Bergs C, Wissenbach U, Flockerzi V, and Trost C (2001). Competitive regulation of CaT-like-mediated Ca2+ entry by protein kinase C and calmodulin. Proc Natl Acad Sci U S A 98, 3600–3605. [PubMed: 11248124]

Nijenhuis T, Hoenderop JG, Nilius B, and Bindels RJ (2003). (Patho)physiological implications of the novel epithelial Ca2+ channels TRPV5 and TRPV6. Pflugers Arch 446, 401–409. [PubMed: 12748856]

Nilius B, Prenen J, Hoenderop JG, Vennekens R, Hoefs S, Weidema AF, Droogmans G, and Bindels RJ (2002). Fast and slow inactivation kinetics of the Ca2+ channels ECaC1 and ECaC2 (TRPV5 and TRPV6). Role of the intracellular loop located between transmembrane segments 2 and 3. J Biol Chem 277, 30852–30858. [PubMed: 12077127]

Owsianik G, Talavera K, Voets T, and Nilius B (2006). Permeation and selectivity of TRP channels. Annu Rev Physiol 68, 685–717. [PubMed: 16460288]

Paulsen CE, Armache JP, Gao Y, Cheng Y, and Julius D (2015). Structure of the TRPA1 ion channel suggests regulatory mechanisms. Nature 520, 511–517. [PubMed: 25855297]

Payandeh J, Scheuer T, Zheng N, and Catterall WA (2011). The crystal structure of a voltage-gated sodium channel. Nature 475, 353–358. [PubMed: 21743477]

Peacock M (2010). Calcium metabolism in health and disease. Clin J Am Soc Nephrol 5 Suppl 1, S23–30.

Peng JB, Chen XZ, Berger UV, Vassilev PM, Tsukaguchi H, Brown EM, and Hediger MA (1999). Molecular cloning and characterization of a channel-like transporter mediating intestinal calcium absorption. J Biol Chem 274, 22739–22746. [PubMed: 10428857]

Peng JB, Chen XZ, Berger UV, Weremowicz S, Morton CC, Vassilev PM, Brown EM, and Hediger MA (2000). Human calcium transport protein CaT1. Biochem Biophys Res Commun 278, 326–332. [PubMed: 11097838]

Peng JB, Suzuki Y, Gyimesi G, and Hediger MA (2018). TRPV5 and TRPV6 Calcium-Selective Channels. In Calcium Entry Channels in Non-Excitable Cells, Kozak JA, and Putney JW Jr., eds. (Boca Raton (FL)), pp. 241–274.

Peng JB, Zhuang L, Berger UV, Adam RM, Williams BJ, Brown EM, Hediger MA, and Freeman MR (2001). CaT1 expression correlates with tumor grade in prostate cancer. Biochem Biophys Res Commun 282, 729–734. [PubMed: 11401523]

Pike JW, Zella LA, Meyer MB, Fretz JA, and Kim S (2007). Molecular actions of 1,25-dihydroxyvitamin D3 on genes involved in calcium homeostasis. J Bone Miner Res 22 Suppl 2, V16–19. [PubMed: 18290714]

Pumroy RA, Samanta A, Liu Y, Hughes TE, Zhao S, Yudin Y, Rohacs T, Han S, and Moiseenkova-Bell VY (2019). Molecular mechanism of TRPV2 channel modulation by cannabidiol. Elife 8.

Qin N, Olcese R, Bransby M, Lin T, and Birnbaumer L (1999). Ca2+-induced inhibition of the cardiac Ca2+ channel depends on calmodulin. Proc Natl Acad Sci U S A 96, 2435–2438. [PubMed: 10051660]

Robertson WG, and Marshall RW (1979). Calcium measurements in serum and plasma--total and ionized. CRC Crit Rev Clin Lab Sci 11, 271–304. [PubMed: 116800]

Sakipov S, Sobolevsky AI, and Kurnikova MG (2018). Ion Permeation Mechanism in Epithelial Calcium Channel TRVP6. Sci Rep 8, 5715. [PubMed: 29632318]

Saotome K, Singh AK, Yelshanskaya MV, and Sobolevsky AI (2016). Crystal structure of the epithelial calcium channel TRPV6. Nature 534, 506–511. [PubMed: 27296226]

Schmiege P, Fine M, Blobel G, and Li X (2017). Human TRPML1 channel structures in open and closed conformations. Nature 550, 366–370. [PubMed: 29019983]

Schwarz EC, Wissenbach U, Niemeyer BA, Strauss B, Philipp SE, Flockerzi V, and Hoth M (2006). TRPV6 potentiates calcium-dependent cell proliferation. Cell Calcium 39, 163–173. [PubMed: 16356545]

Semenova SB, Vassilieva IO, Fomina AF, Runov AL, and Negulyaev YA (2009). Endogenous expression of TRPV5 and TRPV6 calcium channels in human leukemia K562 cells. Am J Physiol Cell Physiol 296, C1098–1104. [PubMed: 19295174]

Shen H, Zhou Q, Pan X, Li Z, Wu J, and Yan N (2017). Structure of a eukaryotic voltage-gated sodium channel at near-atomic resolution. Science 355.

Shen PS, Yang X, DeCaen PG, Liu X, Bulkley D, Clapham DE, and Cao E (2016). The Structure of the Polycystic Kidney Disease Channel PKD2 in Lipid Nanodiscs. Cell 167, 763–773 e711. [PubMed: 27768895]

Simonin C, Awale M, Brand M, van Deursen R, Schwartz J, Fine M, Kovacs G, Hafliger P, Gyimesi G, Sithampari A, et al. (2015). Optimization of TRPV6 Calcium Channel Inhibitors Using a 3D Ligand-Based Virtual Screening Method. Angew Chem Int Ed Engl 54, 14748–14752. [PubMed: 26457814]

Singh AK, McGoldrick LL, Demirkhanyan L, Leslie M, Zakharian E, and Sobolevsky AI (2019). Structural basis of temperature sensation by the TRP channel TRPV3. Nat Struct Mol Biol 26, 994–998. [PubMed: 31636415]

Singh AK, McGoldrick LL, and Sobolevsky AI (2018a). Structure and gating mechanism of the transient receptor potential channel TRPV3. Nat Struct Mol Biol 25, 805–813. [PubMed: 30127359]

Singh AK, McGoldrick LL, Twomey EC, and Sobolevsky AI (2018b). Mechanism of calmodulin inactivation of the calcium-selective TRP channel TRPV6. Sci Adv 4, eaau6088. [PubMed: 30116787]

Singh AK, Saotome K, McGoldrick LL, and Sobolevsky AI (2018c). Structural bases of TRP channel TRPV6 allosteric modulation by 2-APB. Nat Commun 9, 2465. [PubMed: 29941865]

Singh AK, Saotome K, and Sobolevsky AI (2017). Swapping of transmembrane domains in the epithelial calcium channel TRPV6. Sci Rep 7, 10669. [PubMed: 28878326]

Song Y, Peng X, Porta A, Takanaga H, Peng JB, Hediger MA, Fleet JC, and Christakos S (2003). Calcium transporter 1 and epithelial calcium channel messenger ribonucleic acid are differentially regulated by 1,25 dihydroxyvitamin D3 in the intestine and kidney of mice. Endocrinology 144, 3885–3894. [PubMed: 12933662]

Su Q, Hu F, Ge X, Lei J, Yu S, Wang T, Zhou Q, Mei C, and Shi Y (2018). Structure of the human PKD1-PKD2 complex. Science 361.

Suzuki Y, Chitayat D, Sawada H, Deardorff MA, McLaughlin HM, Begtrup A, Millar K, Harrington J, Chong K, Roifman M, et al. (2018). TRPV6 Variants Interfere with Maternal-Fetal Calcium Transport through the Placenta and Cause Transient Neonatal Hyperparathyroidism. Am J Hum Genet 102, 1104–1114. [PubMed: 29861107]

Suzuki Y, Kovacs CS, Takanaga H, Peng JB, Landowski CP, and Hediger MA (2008a). Calcium channel TRPV6 is involved in murine maternal-fetal calcium transport. J Bone Miner Res 23, 1249–1256. [PubMed: 18348695]

Suzuki Y, Landowski CP, and Hediger MA (2008b). Mechanisms and regulation of epithelial Ca2+ absorption in health and disease. Annu Rev Physiol 70, 257–271. [PubMed: 17850211]

Tang L, Gamal El-Din TM, Payandeh J, Martinez GQ, Heard TM, Scheuer T, Zheng N, and Catterall WA (2014). Structural basis for Ca2+ selectivity of a voltage-gated calcium channel. Nature 505, 56–61. [PubMed: 24270805]

Tang Q, Guo W, Zheng L, Wu JX, Liu M, Zhou X, Zhang X, and Chen L (2018). Structure of the receptor-activated human TRPC6 and TRPC3 ion channels. Cell Res 28, 746–755. [PubMed: 29700422]

Tao X, Hite RK, and MacKinnon R (2017). Cryo-EM structure of the open high-conductance Ca(2+)-activated K(+) channel. Nature 541, 46–51. [PubMed: 27974795]

Taparia S, Fleet JC, Peng JB, Wang XD, and Wood RJ (2006). 1,25-Dihydroxyvitamin D and 25-hydroxyvitamin D--mediated regulation of TRPV6 (a putative epithelial calcium channel) mRNA expression in Caco-2 cells. Eur J Nutr 45, 196–204. [PubMed: 16362534]

Tavani A, Gallus S, Franceschi S, and La Vecchia C (2001). Calcium, dairy products, and the risk of prostate cancer. Prostate 48, 118–121. [PubMed: 11433421]

Tidow H, and Nissen P (2013). Structural diversity of calmodulin binding to its target sites. FEBS J 280, 5551–5565. [PubMed: 23601118]

Togashi K, Inada H, and Tominaga M (2008). Inhibition of the transient receptor potential cation channel TRPM2 by 2-aminoethoxydiphenyl borate (2-APB). Br J Pharmacol 153, 1324–1330. [PubMed: 18204483]

Turnbull CI, Looi K, Mangum JE, Meyer M, Sayer RJ, and Hubbard MJ (2004). Calbindin independence of calcium transport in developing teeth contradicts the calcium ferry dogma. J Biol Chem 279, 55850–55854. [PubMed: 15494408]

Twomey EC, Yelshanskaya MV, Grassucci RA, Frank J, and Sobolevsky AI (2017). Channel opening and gating mechanism in AMPA-subtype glutamate receptors. Nature 549, 60–65. [PubMed: 28737760]

Van Cromphaut SJ, Rummens K, Stockmans I, Van Herck E, Dijcks FA, Ederveen AG, Carmeliet P, Verhaeghe J, Bouillon R, and Carmeliet G (2003). Intestinal calcium transporter genes are upregulated by estrogens and the reproductive cycle through vitamin D receptor-independent mechanisms. J Bone Miner Res 18, 1725–1736. [PubMed: 14584880]

van der Wijst J, Leunissen EH, Blanchard MG, Venselaar H, Verkaart S, Paulsen CE, Bindels RJ, and Hoenderop JG (2017). A Gate Hinge Controls the Epithelial Calcium Channel TRPV5. Sci Rep 7, 45489. [PubMed: 28374795]

Vassilieva IO, Tomilin VN, Marakhova II, Shatrova AN, Negulyaev YA, and Semenova SB (2013). Expression of transient receptor potential vanilloid channels TRPV5 and TRPV6 in human blood lymphocytes and Jurkat leukemia T cells. J Membr Biol 246, 131–140. [PubMed: 23111462]

Velisetty P, Borbiro I, Kasimova MA, Liu L, Badheka D, Carnevale V, and Rohacs T (2016). A molecular determinant of phosphoinositide affinity in mammalian TRPV channels. Sci Rep 6, 27652. [PubMed: 27291418]

Vennekens R, Prenen J, Hoenderop JG, Bindels RJ, Droogmans G, and Nilius B (2001). Pore properties and ionic block of the rabbit epithelial calcium channel expressed in HEK 293 cells. J Physiol 530, 183–191. [PubMed: 11208967]

Vennekens R, Voets T, Bindels RJ, Droogmans G, and Nilius B (2002). Current understanding of mammalian TRP homologues. Cell Calcium 31, 253–264. [PubMed: 12098215]

Vinayagam D, Mager T, Apelbaum A, Bothe A, Merino F, Hofnagel O, Gatsogiannis C, and Raunser S (2018). Electron cryo-microscopy structure of the canonical TRPC4 ion channel. Elife 7.

Voets T, Janssens A, Droogmans G, and Nilius B (2004). Outer pore architecture of a Ca2+-selective TRP channel. J Biol Chem 279, 15223–15230. [PubMed: 14736889]

Voets T, Janssens A, Prenen J, Droogmans G, and Nilius B (2003). Mg2+-dependent gating and strong inward rectification of the cation channel TRPV6. J Gen Physiol 121, 245–260. [PubMed: 12601087]

Voets T, Prenen J, Fleig A, Vennekens R, Watanabe H, Hoenderop JG, Bindels RJ, Droogmans G, Penner R, and Nilius B (2001). CaT1 and the calcium release-activated calcium channel manifest distinct pore properties. J Biol Chem 276, 47767–47770. [PubMed: 11687570]

Wangemann P, Nakaya K, Wu T, Maganti RJ, Itza EM, Sanneman JD, Harbidge DG, Billings S, and Marcus DC (2007). Loss of cochlear HCO3- secretion causes deafness via endolymphatic acidification and inhibition of Ca2+ reabsorption in a Pendred syndrome mouse model. Am J Physiol Renal Physiol 292, F1345–1353. [PubMed: 17299139]

Weissgerber P, Kriebs U, Tsvilovskyy V, Olausson J, Kretz O, Stoerger C, Mannebach S, Wissenbach U, Vennekens R, Middendorff R, et al. (2012). Excision of Trpv6 gene leads to severe defects in epididymal Ca2+ absorption and male fertility much like single D541A pore mutation. J Biol Chem 287, 17930–17941. [PubMed: 22427671]

Weissgerber P, Kriebs U, Tsvilovskyy V, Olausson J, Kretz O, Stoerger C, Vennekens R, Wissenbach U, Middendorff R, Flockerzi V, et al. (2011). Male fertility depends on Ca(2)+ absorption by TRPV6 in epididymal epithelia. Sci Signal 4, ra27. [PubMed: 21540454]

Whicher JR, and MacKinnon R (2016). Structure of the voltage-gated K(+) channel Eag1 reveals an alternative voltage sensing mechanism. Science 353, 664–669. [PubMed: 27516594]

Winkler PA, Huang Y, Sun W, Du J, and Lu W (2017). Electron cryo-microscopy structure of a human TRPM4 channel. Nature 552, 200–204. [PubMed: 29211723]

Wissenbach U, Niemeyer B, Himmerkus N, Fixemer T, Bonkhoff H, and Flockerzi V (2004). TRPV6 and prostate cancer: cancer growth beyond the prostate correlates with increased TRPV6 Ca2+ channel expression. Biochem Biophys Res Commun 322, 1359–1363. [PubMed: 15336984]

Wissenbach U, and Niemeyer BA (2007). Trpv6. Handb Exp Pharmacol, 221–234. [PubMed: 17217060]

Wissenbach U, Niemeyer BA, Fixemer T, Schneidewind A, Trost C, Cavalie A, Reus K, Meese E, Bonkhoff H, and Flockerzi V (2001). Expression of CaT-like, a novel calcium-selective channel, correlates with the malignancy of prostate cancer. J Biol Chem 276, 19461–19468. [PubMed: 11278579]

Wu G, Zhang W, Na T, Jing H, Wu H, and Peng JB (2012). Suppression of intestinal calcium entry channel TRPV6 by OCRL, a lipid phosphatase associated with Lowe syndrome and Dent disease. Am J Physiol Cell Physiol 302, C1479–1491. [PubMed: 22378746]

Wu J, Yan Z, Li Z, Yan C, Lu S, Dong M, and Yan N (2015). Structure of the voltage-gated calcium channel Cav1.1 complex. Science 350, aad2395. [PubMed: 26680202]

Xu X, Ali S, Li Y, Yu H, Zhang M, Lu J, and Xu T (2016). 2-Aminoethoxydiphenyl Borate Potentiates CRAC Current by Directly Dilating the Pore of Open Orai1. Sci Rep 6, 29304. [PubMed: 27373367]

Xue H, Wang Y, MacCormack TJ, Lutes T, Rice C, Davey M, Dugourd D, Ilenchuk TT, and Stewart JM (2018). Inhibition of Transient Receptor Potential Vanilloid 6 channel, elevated in human ovarian cancers, reduces tumour growth in a xenograft model. J Cancer 9, 3196–3207. [PubMed: 30210643]

Yang SS, Lo YF, Yu IS, Lin SW, Chang TH, Hsu YJ, Chao TK, Sytwu HK, Uchida S, Sasaki S, et al. (2010). Generation and analysis of the thiazide-sensitive Na+ -Cl- cotransporter (Ncc/Slc12a3) Ser707X knockin mouse as a model of Gitelman syndrome. Hum Mutat 31, 1304–1315. [PubMed: 20848653]

Yang W, Lee HW, Hellinga H, and Yang JJ (2002). Structural analysis, identification, and design of calcium-binding sites in proteins. Proteins 47, 344–356. [PubMed: 11948788]

Yin Y, Wu M, Zubcevic L, Borschel WF, Lander GC, and Lee SY (2018). Structure of the cold- and menthol-sensing ion channel TRPM8. Science 359, 237–241. [PubMed: 29217583]

Zakharian E, Cao C, and Rohacs T (2011). Intracellular ATP supports TRPV6 activity via lipid kinases and the generation of PtdIns(4,5) P(2). FASEB J 25, 3915–3928. [PubMed: 21810903]

Zhang Z, Toth B, Szollosi A, Chen J, and Csanady L (2018). Structure of a TRPM2 channel in complex with Ca(2+) explains unique gating regulation. Elife 7.

Zheng XE, Wang Z, Liao MZ, Lin YS, Shuhart MC, Schuetz EG, and Thummel KE (2012). Human PXR-mediated induction of intestinal CYP3A4 attenuates 1alpha,25-dihydroxyvitamin D(3) function in human colon adenocarcinoma LS180 cells. Biochem Pharmacol 84, 391–401. [PubMed: 22562045]

Zhou X, Li M, Su D, Jia Q, Li H, Li X, and Yang J (2017). Cryo-EM structures of the human endolysosomal TRPML3 channel in three distinct states. Nat Struct Mol Biol 24, 1146–1154. [PubMed: 29106414]

Zhuang L, Peng JB, Tou L, Takanaga H, Adam RM, Hediger MA, and Freeman MR (2002). Calcium-selective ion channel, CaT1, is apically localized in gastrointestinal tract epithelia and is aberrantly expressed in human malignancies. Lab Invest 82, 1755–1764. [PubMed: 12480925]

Zhuo RG, Liu XY, Zhang SZ, Wei XL, Zheng JQ, Xu JP, and Ma XY (2015). Insights into the stimulatory mechanism of 2-aminoethoxydiphenyl borate on TREK-2 potassium channel. Neuroscience 300, 85–93. [PubMed: 25982558]

Zubcevic L, Borschel WF, Hsu AL, Borgnia MJ, and Lee SY (2019a). Regulatory switch at the cytoplasmic interface controls TRPV channel gating. Elife 8.

Zubcevic L, Herzik MA Jr., Chung BC, Liu Z, Lander GC, and Lee SY (2016). Cryo-electron microscopy structure of the TRPV2 ion channel. Nat Struct Mol Biol 23, 180–186. [PubMed: 26779611]

Zubcevic L, Herzik MA Jr., Wu M, Borschel WF, Hirschi M, Song AS, Lander GC, and Lee SY (2018). Conformational ensemble of the human TRPV3 ion channel. Nat Commun 9, 4773. [PubMed: 30429472]

Zubcevic L, Hsu AL, Borgnia MJ, and Lee SY (2019b). Symmetry transitions during gating of the TRPV2 ion channel in lipid membranes. Elife 8.

Zuhlke RD, Pitt GS, Deisseroth K, Tsien RW, and Reuter H (1999). Calmodulin supports both inactivation and facilitation of L-type calcium channels. Nature 399, 159–162. [PubMed: 10335846]

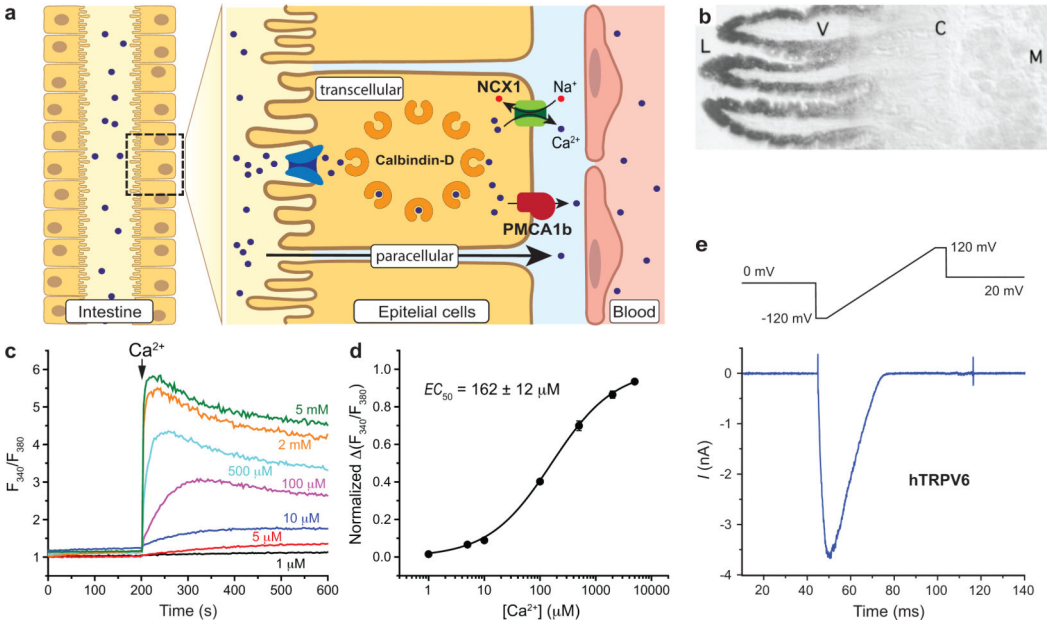

Figure 1. Role in epithelial Ca^{2+} transport and functional properties of TRPV6.

a, TRPV6 mediates the absorption of Ca^{2+} from the intestine as a component of the transcellular epithelial Ca^{2+} transport. Following entry from the intestinal lumen into the epithelial cell through TRPV6, Ca^{2+} bound to calbindin diffuses to the basolateral membrane, where it is extruded to the interstitial space adjacent to the blood vessel by means of ATP-dependent Ca^{2+}-ATPase PMCA1 and Na^{2+}/Ca^{2+} exchanger NCX1. **b**, TRPV6 expression in the rat duodenum. Shown is a bright-field micrograph of a cryosection hybridized to a digoxigenin-labeled TRPV6 antisense cRNA probe (M, muscle layer; V, villi; C, crypt; L, lumen). TRPV6 is expressed in enterocytes lining the villi, with the highest mRNA concentrations at the villi tips. Originally published in (Peng et al., 1999). **c-d**, Functional characterization of hTRPV6 using ratiometric fluorescence measurements. **c**, Fluorescence curves recorded from HEK 293 cells expressing hTRPV6 in response to the application of Ca^{2+} (arrow) at different concentrations. **d**, Ca^{2+} dose-response curve for the maximal value of fluorescence fitted with the logistic equation. Calculated IC_{50} is the mean ± SEM (n = 3). **e,** Whole-cell patch-clamp recording from HEK 293 cells expressing wild type hTRPV6. Shown is a leak-subtracted current in response to the voltage ramp protocol illustrated above the recording. Adapted from (McGoldrick et al., 2018).

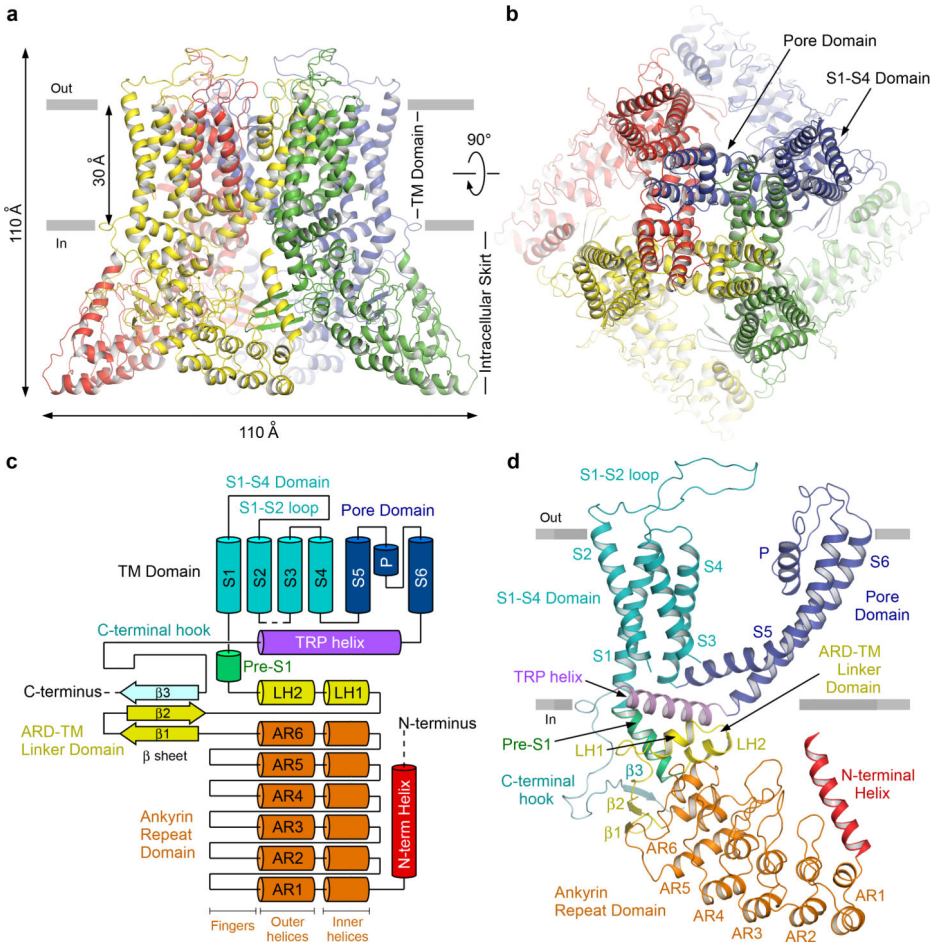

Figure 2. Architecture and domain organization of TRPV6.

a-b, Side (**a**) and top (**b**) views of the human TRPV6 tetramer (PDB ID: 6BO8), with each subunit shown in different color. **c**, Domain organization diagram of the TRPV6 subunit. **d**, A single human TRPV6 subunit, with domains colored similarly to **c**. The diagram in (**c**) and the overall design are adapted from (Saotome et al., 2016).

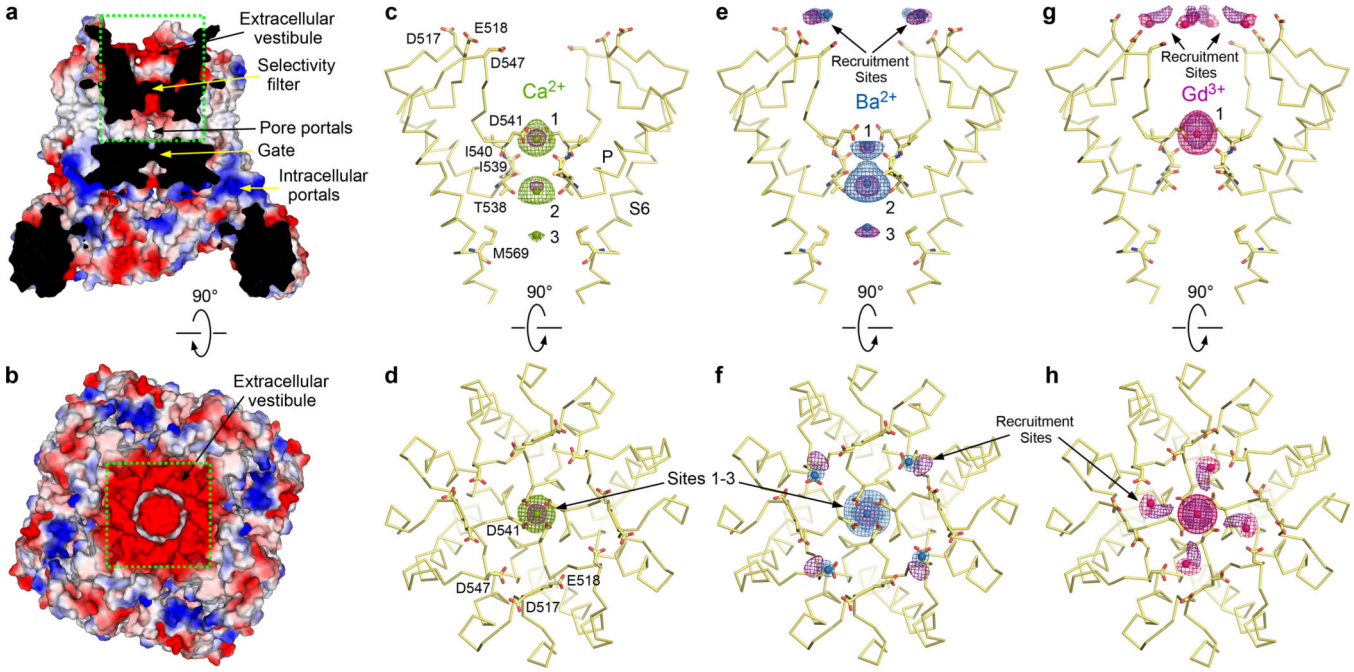

Figure 3. Cation binding sites in the TRPV6 pore.

a-b, Central slice (**a**) and top (**b**) views of crystal structure of rat TRPV6 (PDB ID: 5IWK) in surface representation, colored by electrostatic potential, with blue being positively charged, red negatively charged, and white neutral. **c-h**, Side (**c,e,g**) and top (**d,f,h**) views of the TRPV6 pore (the channel portion indicated by green dashed rectangles in **a-b**), with residues important for cation binding shown in stick representation. Front and back subunits in **c**, **e** and **g** are removed for clarity. Green, blue and pink mesh shows anomalous difference electron density for Ca^{2+} (**c-d**, 38–4.59 Å, 2.7**σ**; PDB ID: 5IWP), Ba^{2+} (**e-f**, 38–4.59 Å, 3.5**σ**; PDB ID: 5IWR) and Gd^{3+} (**g-h**, 38–4.59 Å, 7**σ**; PDB ID: 5IWT) and ions are shown as spheres of the corresponding color. Purple mesh shows simulated-annealing F_O-F_C electron density maps contoured at 4**σ** for Ca^{2+} (50–3.65 Å), 3**σ** for Ba^{2+} (50–3.85 Å) and 3.5**σ** for Gd^{3+} (50–3.80 Å). Adapted from (Saotome et al., 2016).

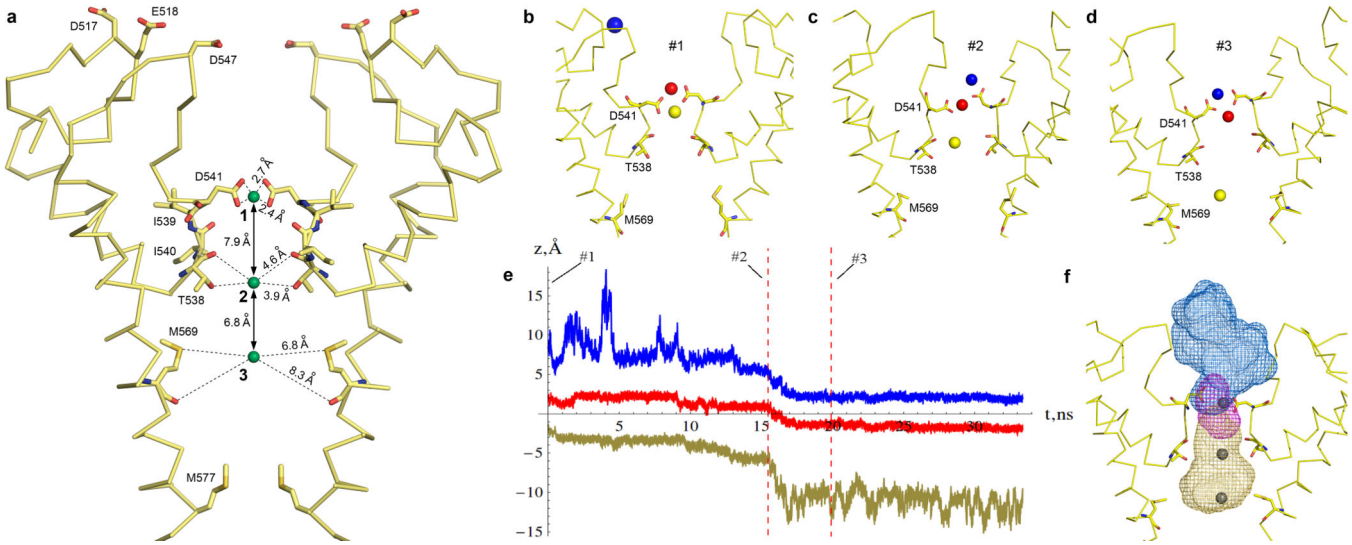

Figure 4. Knock-off mechanism of Ca^{2+} permeation.

a, Side view of rat TRPV6 (PDB ID: 5IWK) pore, with front and back subunits removed for clarity. Residues that surround or contribute to cation binding sites are shown as sticks, and Ca^{2+} ions at Sites 1, 2 and 3 are shown as green spheres. The interatomic distances illustrated by dashed lines suggest that Ca^{2+} is directly coordinated by D541 side chains at Site 1, while a hydrated Ca^{2+} ion indirectly interacts with the pore at Sites 2 and 3. **b-f**, Molecular dynamics simulation of calcium permeation through the selectivity filter. **b-d**, Sequential representative positions of Ca^{2+} ions in its initial (**b**, #1), transition (**c**, #2) and final (**d**, #3) configurations. Blue, magenta and mustard colored spheres represent an incoming, intermediate and leaving Ca^{2+} ions, respectively. Residues D541, T538, and M569 are shown in stick representation. **e**, Positions of ions along the z-axis. The positions #1, #2 and #3 correspond to the configurations of ions shown in **b**, **c** and **d**, respectively. **f**, Spaces occupied by each of the three calcium ions throughout the entire simulation, shown as mesh surfaces colored similarly to ions in **b-d**. Adapted from (Saotome et al., 2016) (**a**) and (Sakipov et al., 2018) (**b-f**).

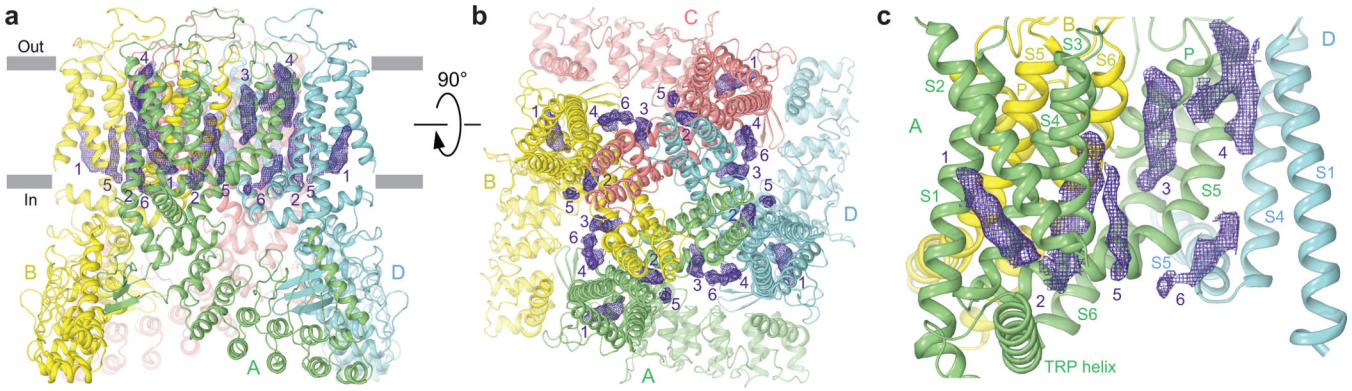

Figure 5. Putative lipid densities.

a-b, Side (**a**) and top (**b**) views of hTRPV6 tetramer (PDB ID: 6BO8), with each subunit (A-D) shown in different color. Putative lipid densities are illustrated by purple mesh and numbered. **c**, Expanded view of the putative lipid densities per hTRPV6 subunit. Adapted from (McGoldrick et al., 2018).

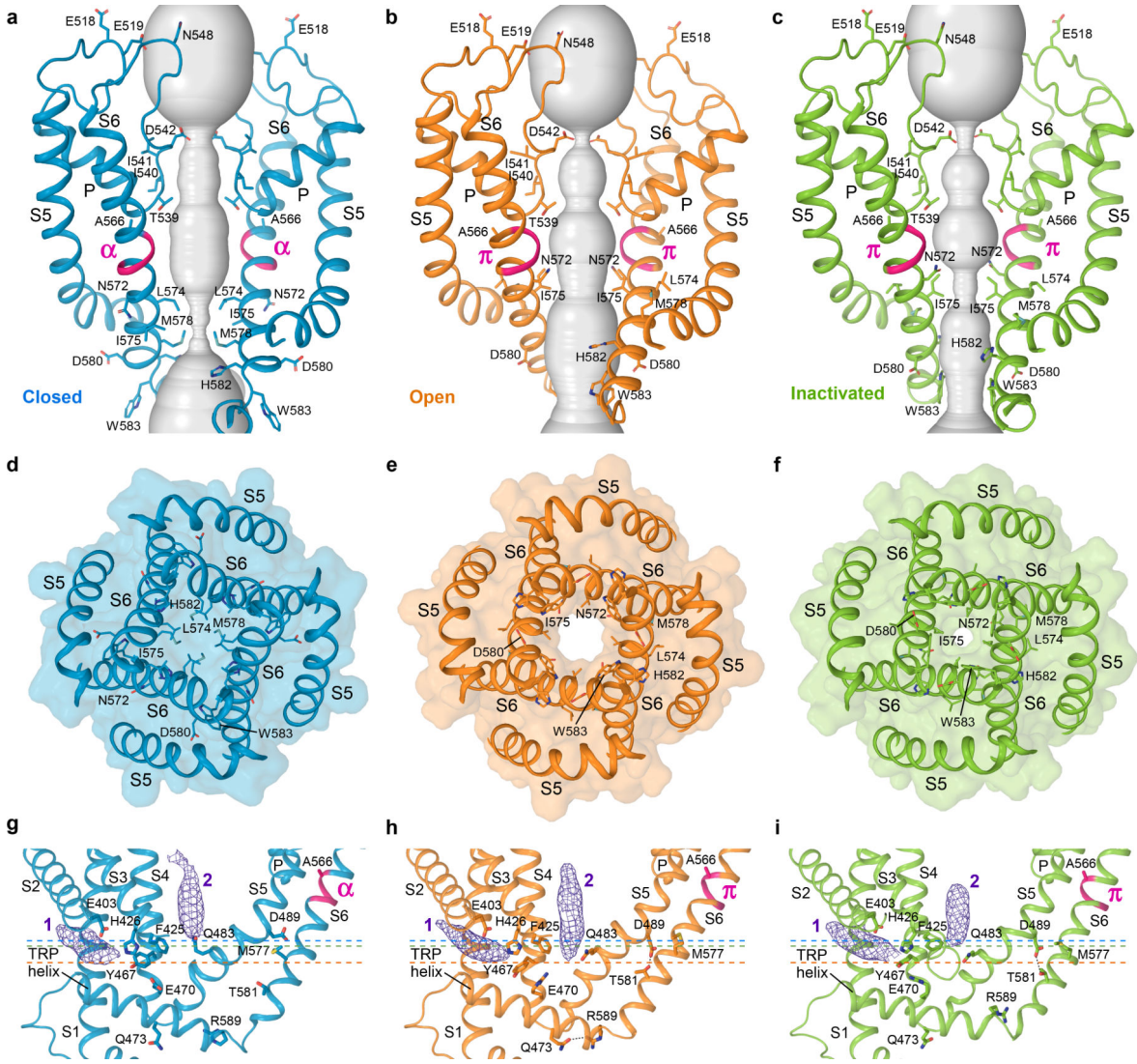

Figure 6. Ion channel pore in the closed, open and inactivated states.

a-c, Ion conduction pathway (grey) in the closed (**a**, hTRPV6-R470E; PDB ID: 6BOA; blue), open (**b**, hTRPV6; PDB ID: 6BO8; orange) and inactivated (**c**, hTRPV6-CaM; PDB ID: 6E2F; green) states, with residues lining the selectivity filter and around the gate shown as sticks. Only two of four subunits are shown, with the front and back subunits removed for clarity. The segment of S6 that undergoes the α-to-π helical transition is highlighted in pink. **d-f**, Intracellular view of the S6 bundle crossing in the closed (**d**), open (**e**) and inactivated (**f**) states, with the surface shown in the corresponding color. **g-i**, Close-up view on putative lipid densities 1 and 2 shown as a purple mesh in the closed (**g**), open (**h**) and inactivated (**i**) states. Residues involved in TRPV6 gating and regulation are shown as sticks. Black dashed lines indicate bonds between residues D489 and T581 as well as Q473 and R589; blue, orange and green horizontal dashed lines indicate the lowest (most intracellular) levels reached by density 2 in the closed, open and inactivated states, respectively. Adapted from (McGoldrick et al., 2018).

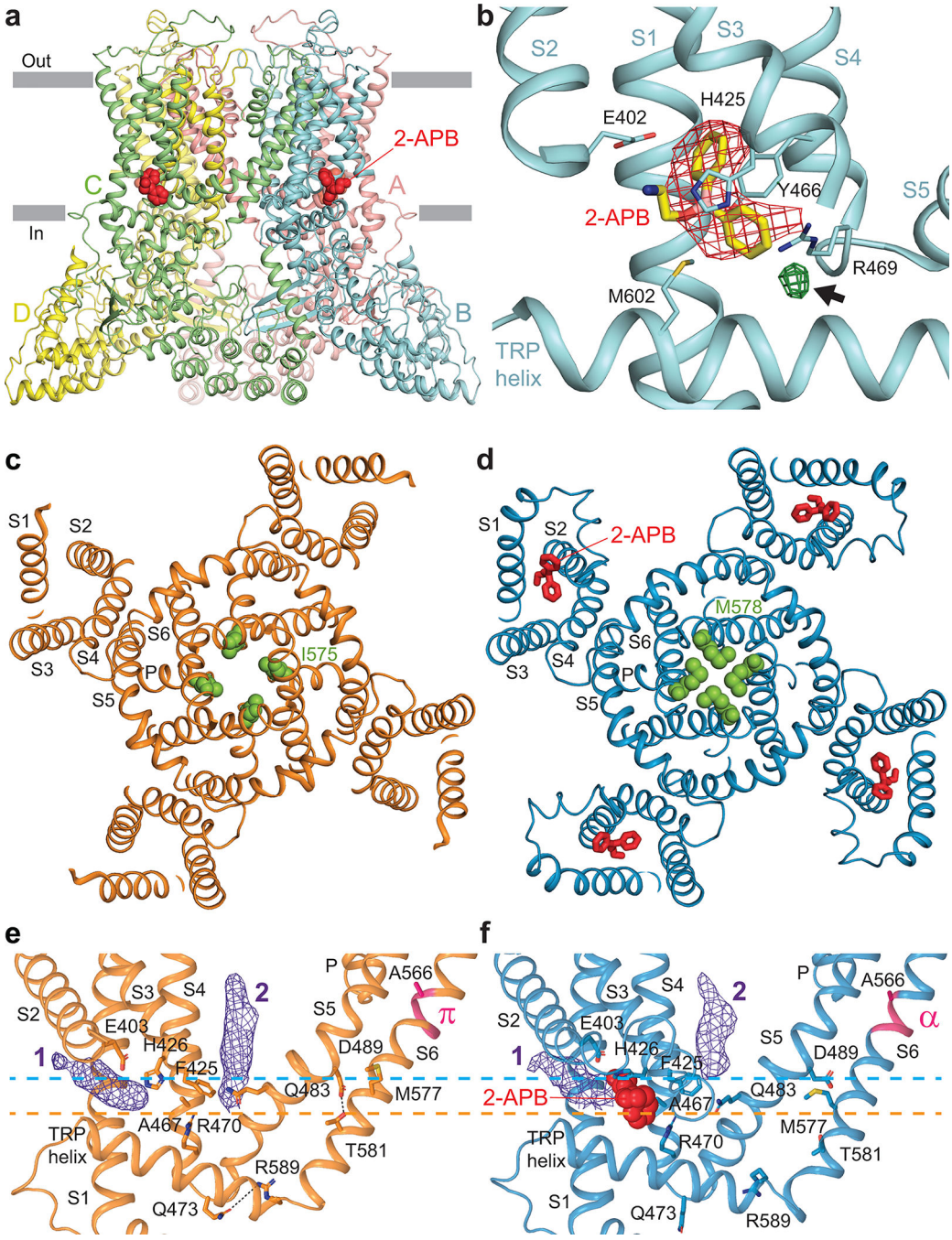

Figure 7. Inhibition of TRPV6 by 2-APB.

a, Side view of rat TRPV6* crystal structure in complex with 2-APB (PDB ID: 6D7O). The molecules of 2-APB are shown as red space-filling models. Four TRPV6* subunits are colored pink, cyan, green and yellow. **b**, Close-up view of the 2-APB binding site with 2-APB (yellow) and surrounding residues shown as sticks. Red mesh shows positive electron density for 2-APB in the F_O-F_C omit map contoured at 3**σ**. Green mesh indicated by the arrow shows electron density for the brominated derivative of 2-APB (2-APB-Br; PDB ID: 6D7V) in the anomalous difference Fourier map contoured at 3**σ**. **c-d**, Intracellular view of

the transmembrane domain in the cryo-EM structures of hTRPV6-Y467A (**c**, PDB ID: 6D7S) and hTRPV6-Y467A$_{2\text{-APB}}$ (**d**, PDB ID: 6D7T). Residues forming the narrowest part of the pore in the gate region, I575 in hTRPV6-Y467A (**c**) and M578 in hTRPV6-Y467A$_{2\text{-APB}}$ (**d**), are shown as space-filling models (green). Molecules of 2-APB are shown as sticks (red). **e-f**, Close-up views of the transmembrane domain of a single subunit in the cryo-EM structures of hTRPV6-Y467A (**e**) and hTRPV6-Y467A$_{2\text{-APB}}$ (**f**) viewed parallel to the membrane. The molecule of 2-APB is shown as a space-filling model (red). Purple mesh shows lipid densities 1 and 2. Black dashed lines indicate bonds between residues D489 and T581 as well as Q473 and R589; horizontal dashed lines indicate the lowest (most intracellular) levels reached by density 2 in the presence (blue) and absence (orange) of 2-APB. The segment of S6 that undergoes the α-to-π helical transition is highlighted in pink. Adapted from (Singh et al., 2018c).

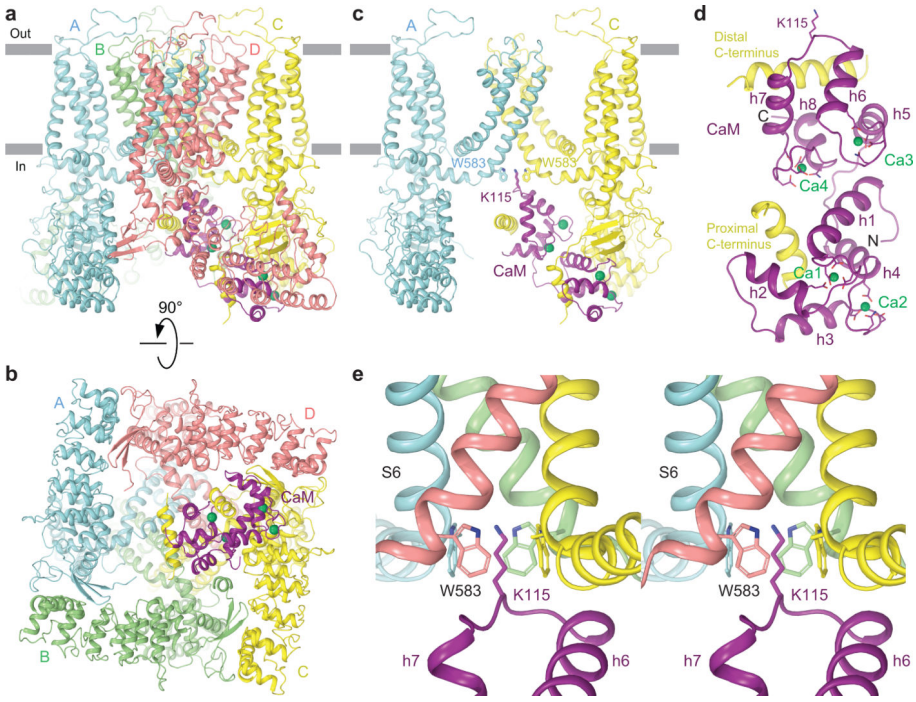

Figure 8. Structure of TRPV6-CaM complex.

a-c, Side (**a, c**), and bottom (**b**) views of hTRPV6-CaM (PDB ID: 6E2F) with hTRPV6 subunits (A-D) colored cyan, green, yellow and pink and CaM colored purple. Calcium ions are shown as green spheres. In (**c**) only two of four subunits are shown, with the front and back subunits being removed for clarity. Side chains of TRPV6 residues W583 and CaM residue K115 are shown as sticks. **d**, Expanded view of CaM bound to the proximal and distal portions of the TRPV6 C-terminus. Side chains of CaM residues coordinating calcium ions and of K115 are shown as sticks. **e,** Stereo view of the intracellular entrance to the channel pore where lysine K115 of CaM forms a unique cation-**π** interaction with tetratryptophan cage assembled of W583, one from each TRPV6 subunit. Adapted from (Singh et al., 2018b).

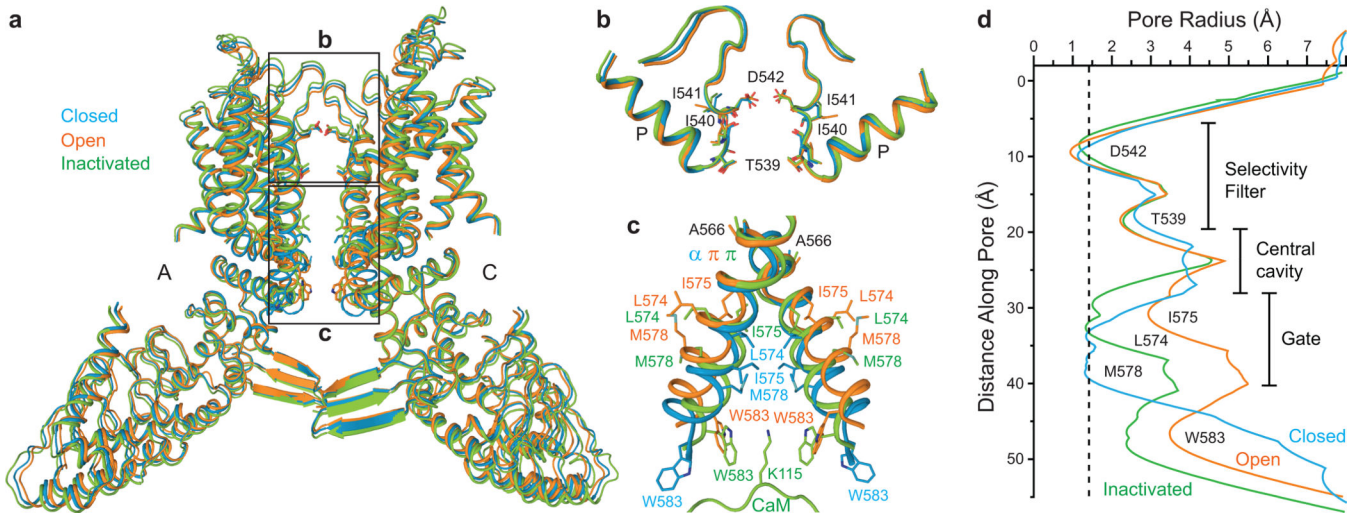

Figure 9. Gating-associated conformational changes.

a-c, Superposition of the full-size hTRPV6 (**a**), its selectivity filter (**b**) and lower pore (**c**) regions in the closed (cyan, hTRPV6-R470E, PDB ID: 6BOA), open (orange, hTRPV6, PDB ID: 6BO8) and inactivated (green, hTRPV6-CaM, PDB ID: 6E2F) states, viewed parallel to membrane. Only two (A and C) of four subunits are shown, with the back (B) and front (D) subunits removed for clarity. Residues lining the selectivity filter, around the gate and lysine K155 of CaM are shown as sticks. Note, the overall shape of the tetramer is very similar in the three states (**a-b**), while the strongest conformational changes are localized in the lower pore region (**c**). **d**, Pore radius calculated for the three states, with the dashed line indicating 1.4 Å (radius of a water molecule). Adapted from (Singh et al., 2018b).

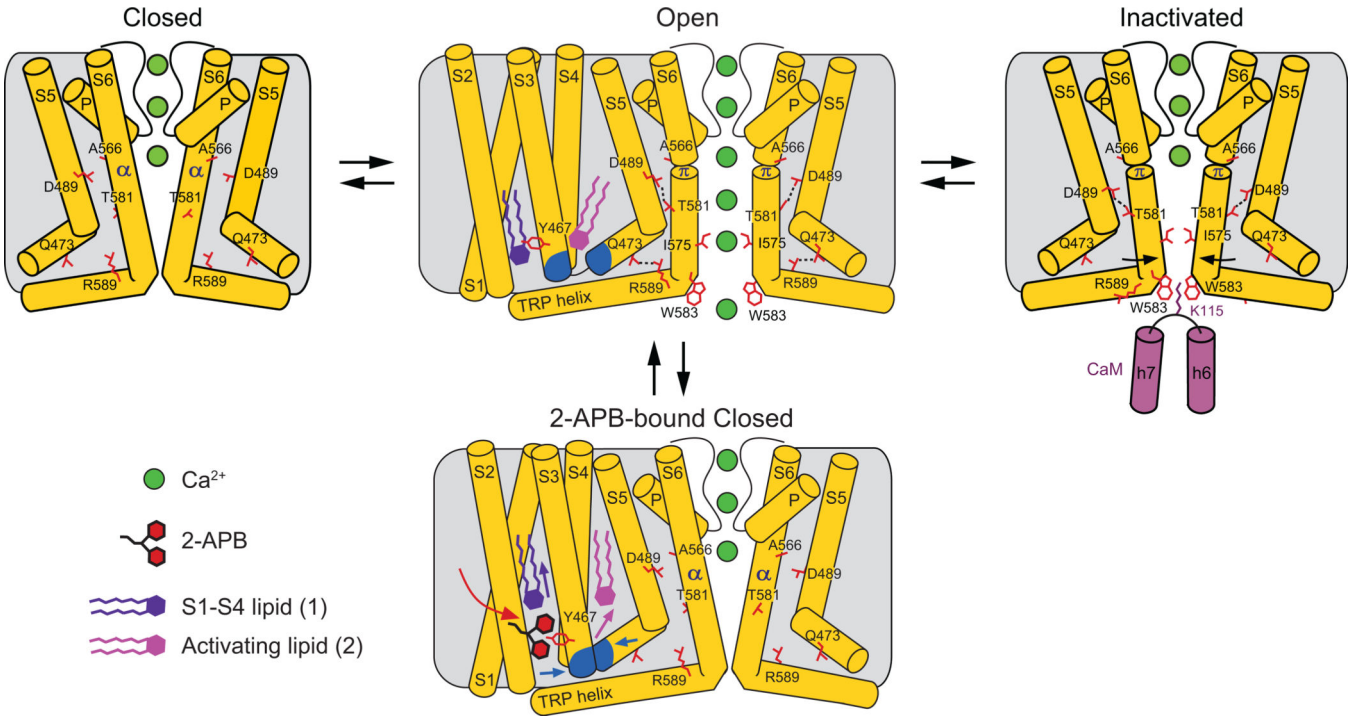

Figure 10. Mechanisms of TRPV6 gating and regulation.

Cartoons represent TRPV6 in the closed, open, inactivated and 2-APB-inhibited closed states. Transition from the closed to open state, stabilized by the formation of salt bridges (dashed lines), leads to permeation of ions (green spheres) and is accompanied by a local α-to-π helical transition in S6 that maintains the selectivity filter conformation, while the lower part of S6 bends by ~11° and rotates by ~100°. These movements result in a different set of residues lining the pore around the channel gate. When 2-APB binds at the base of the S1-S4 bundle, it displaces the putative lipid 1 (purple) and promotes formation of the hydrophobic cluster (blue). Formation of the cluster displaces the putative activating lipid 2 (pink) and breaks hydrogen bonds (dashed lines), which stabilize the open state by energetically compensating the unfavorable α-to-π helical transition in S6. As S6 turns α-helical, the channel closes and its pore becomes impermeable to ions. The transition from the open to the inactivated state involves tilting of the lower portions of the S6 helices towards the center of the pore at the alanine A566 gating hinge and closure of the pore. The loss of the R589-Q473 salt bridges, which stabilize the α-to-π helical transition in S6 in the open state, is compensated by a cation-π interaction between K115 and the π-system of four tryptophans W583 forming a cage at the pore intracellular entrance.